UFMylation and TRAMP-like complexes are required for hepatitis A virus pathogenesis

Jessie Kulsuptrakul[1], Ruofan Wang[1], Nathan L. Meyers[2], Melanie Ott[2], Andreas S. Puschnik[1,*]

[1] Chan Zuckerberg Biohub, San Francisco, United States

[2] Gladstone Institutes, University of California San Francisco, San Francisco, United States

For correspondence: andreas.puschnik@czbiohub.org

Abstract

Hepatitis A virus (HAV) is a positive-sense RNA virus causing acute inflammation of the liver. Here, using a genome-scale CRISPR screen in a human hepatocyte cell line, we provide a comprehensive picture of the cellular factors, which are exploited by HAV during replication. We identified genes involved in sialic acid and ganglioside biosynthesis, the eukaryotic initiation factor complex and the ESCRT pathway. Additionally, we found all components of the cellular machinery for UFMylation, a ubiquitin-like protein modification, and showed that optimal translation of the HAV genome depends on UFM1 conjugation of the ribosomal protein RPL26. Furthermore, we demonstrated that components related to the yeast Trf4/5–Air1/2–Mtr4 polyadenylation (TRAMP) complex, are required for viral translation, independent of regulating HAV poly(A) tails. Finally, pharmacological inhibition of the TRAMP-like complex decreased HAV replication in hepatocyte cells and human liver organoids, thus providing a strategy for host-directed therapy of HAV infection.

22 **Introduction**

23 Hepatitis A virus (HAV) is a single-stranded, positive-sense RNA virus and a hepatotropic member
24 of the *Picornaviridae*. Despite successes in vaccine development, HAV remains a common cause
25 of enterically transmitted hepatitis globally, responsible for epidemics in developing and
26 developed countries with symptoms ranging from mild inflammation and jaundice to acute liver
27 failure (CDC, 2019; Jacobsen, 2018). HAV enters host cells through interactions with cell surface
28 molecules, followed by uncoating and delivery of viral RNA from endosomes to the cytosol. The
29 viral polyprotein is synthesized under the control of an internal ribosome entry site (IRES) and
30 processed into the individual structural and non-structural proteins. HAV then co-opts cellular
31 membranes to form organelle-like structures, where viral genome replication occurs. The newly
32 synthesized genomes are packaged and HAV egresses in the form of quasi-enveloped virions
33 (McKnight and Lemon, 2018). Despite a general understanding of the life cycle and
34 characterization of certain host proteins involved during replication, a comprehensive overview
35 of the most critical host factors for HAV infection is lacking. CRISPR screens are a powerful
36 technology to interrogate cell components critical for viral infection in an unbiased fashion and
37 have been used to study human pathogens, such as mosquito-borne flaviviruses, enteroviruses
38 or hepatitis C virus (Diep et al., 2019; Marceau et al., 2016; Zhang et al., 2016). Using this
39 approach to dissect HAV infection, we identified previously known and unknown host factors and
40 highlight that HAV co-opts pathways distinct from other *Picornaviridae* members. Additionally,
41 we reveal a strategy for host-directed therapy of HAV infections.

42

43

44 **Results**

45 To identify host cellular factors that are critical for HAV infection, we conducted a genome-wide
46 CRISPR knockout (KO) screen in the human hepatocyte cell line Huh7.5.1 using the cytopathic
47 HAV HM175/18f strain (Lemon et al., 1991) (Figure 1A). Infection led to notable cell death after
48 ~3 days and surviving cells were collected after 12 days for analysis. We consistently found
49 enrichment of guide RNA (gRNA) sequences targeting genes involved in several pathways known
50 to be required for picornaviral replication (Figure 1B, Figure 1-figure supplement 1A, Figure 1-
51 source data 1). For example, sialic acid and ganglioside biosynthesis genes (*GNE, CMAS, SLC35A1,*
52 *UGCG, ST3GAL5*) were previously implicated in entry of picorna- and other viruses (Baggen et al.,
53 2016; Ding et al., 2018; Drake et al., 2017; Han et al., 2018). We also identified *PTBP1* and
54 members of the eukaryotic initiation factor complex (*EIF4B, EIF3C, EIF3CL*), which have known
55 roles in IRES-mediated translation of HAV and other picornaviruses (Avanzino et al., 2017;
56 Borman et al., 2001; Gosert et al., 2000; Pestova et al., 1996). VPS4A is an endosomal sorting
57 complexes required for transport (ESCRT) component, important for budding of several
58 enveloped viruses as well as egress of HAV (Feng et al., 2013; Votteler and Sundquist, 2013).
59 Importantly, gene ontology (GO) analysis of enriched genes (RIGER p-value < 0.001) revealed
60 additional pathways, which have not previously been implicated in HAV infection, such as the
61 machinery for UFMylation (*UFM1, UBA5, UFL1, UFC1, UFSP2*), a ubiquitin-like protein
62 modification (Gerakis et al., 2019; Komatsu et al., 2004), and the TRAMP complex components
63 PAPD5 (also known as TENT4B or TRF4-2) and PAPD7 (also known as TENT4A or TRF4-1) (Figure
64 1B and C and Figure 1-source data 2) (Lubas et al., 2011; Warkocki et al., 2018). Zinc Finger CCHC
65 Domain-Containing Protein 14 (ZCCHC14), which has been shown to associate with PAPD7 using

66 BioID, is likely to be part of a TRAMP-like complex, which generally contains a zinc knuckle protein
67 (Go et al., 2019; Hamill et al., 2010).

68 We systematically compared our hits with CRISPR screens for host factors of human
69 rhinovirus C15 (HRV-C15) and enterovirus D68 (EV-D68), two distantly related *Picornaviridae*
70 members (Figure 1-figure supplement 1B) (Diep et al., 2019). Other than sialic acid biosynthesis
71 genes among the EV-D68 hits, there were no commonalities, indicating divergent evolution of
72 host factor dependencies (Figure 1-figure supplement 1C and D). Additionally, we compared our
73 results to a CRISPR screen for hepatitis C virus (HCV) infection, another hepatotropic positive-
74 sense RNA virus (and member of the *Flaviviridae* family) but found no overlap in the host factor
75 requirements (Figure 1-figure supplement 1E) (Marceau et al., 2016).

76 To validate the results of our screen, we generated isogenic KO cell lines in several genes
77 by CRISPR-Cas9 gene editing resulting in loss of protein expression (Figure 2-figure supplement
78 1A-C). Upon HAV infection, we observed significant reduction of both intra- and extracellular viral
79 RNA (ranging from 10-1,000 fold) relative to levels in wild-type (WT) cells at 72 hours post-
80 infection (hpi) (Figure 2A and Figure 2-figure supplement 2A). As PAPD5 and PAPD7 are both
81 human orthologues of yeast Trf4p and display redundancy in their polyadenylation function
82 (Warkocki et al., 2018), we generated *PAPD5/PAPD7* double knockout (DKO) cell lines (Figure 2-
83 figure supplement 1A). We observed a significantly stronger reduction in viral replication in the
84 DKO cells compared to the single *PAPD5* or *PAPD7* KO cells underscoring their redundant activity
85 for HAV replication (Figure 2B). To rule out that phenotypes are not only observed with the highly
86 tissue culture adapted HM175/18f strain, we additionally performed infection assays in KO cell
87 lines using a lower-passage HM175 strain with similar results (Figure 2-figure supplement 2B).

88 Next, we performed a timecourse infection assay using a recombinant reporter virus that
89 expresses nanoluciferase from within its polyprotein (HAV-NLuc). We measured a ~10^4 fold
90 increase in luminescence in WT cells after 72hpi but there was striking attenuation of luciferase
91 expression in host factor KO lines (Figure 2C). Moreover, when we complemented *UBA5*, *PAPD5*
92 and *ZCCHC14* KO cells with the respective cDNAs, we observed a significant increase in HAV RNA
93 levels (Figure 2D-F and Figure 2-figure supplement 1C).

94 Next, we compared replication of different *Picornaviridae* members in *UFM1* KO cells. As
95 expected, HAV RNA levels were greatly reduced while enterovirus 71 (EV-71) and
96 encephalomyocarditis virus (EMCV) RNA levels were not affected (Figure 2G). Interestingly,
97 human rhinovirus A2 (RV-A2) replication was increased suggesting that UFMylation can mediate
98 pro- and antiviral functions in host cells, depending on the virus species. In cells deficient in both
99 PAPD5 and PAPD7, HAV RNA levels were severely and EMCV RNA levels moderately decreased
100 while EV-71 and RV-A2 replication were unaffected (Figure 2H).

101 It is of note that our screen did not reveal HAVCR1 (also known as TIM1) as an essential
102 host factor for HAV infection. HAVCR1 was originally identified as a HAV receptor but a more
103 recent study questioned its essentiality for HAV infection (Das et al., 2017; Kaplan et al., 1996).
104 To address this further, we generated isogenic *HAVCR1* KO lines (Figure 2-figure supplement 1A)
105 and performed a viral attachment and internalization assay. We only observed a minor defect of
106 internalized virions at 6hpi and viral RNA levels were only reduced by ~2 fold relative to WT cells
107 at 30hpi (Figure 2-figure supplement 3). Thus, *HAVCR1* KO cells were unlikely to be protected
108 against cytopathic HAV infection in the CRISPR screen. By contrast, in *SLC35A1* KO cells
109 intracellular viral RNA was decreased by ~80% at 6hpi and ~95% at 30hpi. We conclude that

110 *HAVCR1* is not essential for the HAV life cycle, while sialic acid biosynthesis is critical for viral
111 entry and establishing infection. Together, these data confirm that the genes identified by the
112 CRISPR screen play an important role in the HAV life cycle.
113
114 *UFM1* encodes the 85 amino acid long ubiquitin-fold modifier 1, which acts as a protein
115 modification and is conserved among most eukaryotes except for yeast and other fungi (Komatsu
116 et al., 2004). Like ubiquitination, UFM1 is covalently attached to its targets following an E1–E2–
117 E3 reaction consisting of the UFM1-activating enzyme UBA5, the UFM1-conjugating enzyme
118 UFC1 and the UFM1-specific ligase UFL1 (Figure 3A) (Komatsu et al., 2004; Tatsumi et al., 2010).
119 Usually, UFM1 is present in a precursor form, which first requires cleavage of the last two C-
120 terminal amino acids by the UFM1-specific protease UFSP2 to expose Gly at position 83 (Komatsu
121 et al., 2004). UFSP2 also operates as the major de-UFMylation enzyme, removing UFM1
122 molecules from their targets (Kang et al., 2007). Our screen identified all known components of
123 the UFMylation machinery including the additionally associated proteins DDRGK1 and ODR4
124 (encoded by *C1orf27*) (Figure 3A) (Chen et al., 2014; Wu et al., 2010). To date, this protein
125 modification has not been implicated to play a role in viral infections. WT cells contain free UFM1
126 as well as conjugated UFM1 as detected by immunoblot (Figure 3B). To probe whether functional
127 conjugation of UFM1 is required for HAV infection, we mutated different components of the
128 pathway. Deletion of UBA5 led to an absence of conjugated UFM1, while UFSP2 KO resulted in
129 hyper-conjugation (Figure 3B). However, both conditions led to a stark reduction of viral RNA in
130 infected cells, suggesting that the modification needs to be reversible for its proviral function
131 (Figure 3C). Moreover, we generated cell lines either lacking UFM1 completely or expressing WT

132 UFM1, Gly83Ala UFM1 or ΔC3 UFM1 (lacking the last 3 C-terminal amino acids) and showed the
133 presence of conjugated UFM1 in cells containing WT UFM1, hyper-conjugation with Gly83Ala
134 UFM1 and absence of UFM1 linkage for ΔC3 UFM1 consistent with previous findings (Figure 3B)
135 (Komatsu et al., 2004). Complementation with WT UFM1 significantly restored HAV replication,
136 although less than the hyper-conjugated Gly83Ala UFM1, possibly because the Gly83Ala mutant
137 may be more stable due to resistance to UFM1 processing (Figure 3C). By contrast, conjugation-
138 deficient ΔC3 UFM1 did not rescue viral infection indicating that functional UFM1 conjugation is
139 indeed critical for HAV (Figure 3C). Complementation of *UBA5* KO cells with WT UBA5 but not
140 catalytically inactive enzyme also restored UFM1 conjugation and viral replication (Figure 3B and
141 Figure 3-figure supplement 1A and B).

142 Next, we used HAV replicon RNA expressing firefly luciferase to assess whether the defect
143 occurs during the viral translation or genome replication step and detected a marked defect in
144 *UBA5, UFSP2* as well as *UFM1* KO cells within 10h post-electroporation (Figure 3D and Figure 3-
145 figure supplement 2A). To specifically measure the effect on translation of incoming viral RNA,
146 we additionally used a replication-incompetent replicon (containing a GDD→GAA mutation in
147 the viral polymerase) and observed a decrease of luciferase expression in all KO cells (Figure 3E
148 and Figure 3-figure supplement 2B). We excluded that observed phenotypes were due to
149 differences in cell viability or proliferation post-electroporation (Figure 3-figure supplement 2C).
150 Thus, we conclude that functional and reversible conjugation of UFM1 is required for optimal
151 translation of HAV RNA.

152 To explore further whether a cellular or viral protein is UFMylated upon infection, we
153 performed immunoblot analysis. We did not observe an additional UFM1 conjugate upon

154 infection, suggesting that a viral protein is not the direct target of UFMylation (Figure 3F).
155 Recently, the ribosomal protein RPL26 was identified as a major target for UFMylation in human
156 cells (Walczak et al., 2019; Wang et al., 2019). Thus, we sought to test whether UFMylated RPL26
157 is important for efficient HAV translation. Consistent with previous findings, we detected
158 modified RPL26 at the molecular weight corresponding to UFM1 conjugates (Figure 3F).
159 Interestingly, only a small fraction of RPL26 is UFMylated and the conjugation appears transient
160 as it can only be visualized in *UFSP2* KO cells, which lack de-UFMylation activity. It was further
161 shown that conjugation of UFM1 occurs at C-terminal lysines of RPL26 (Walczak et al., 2019;
162 Wang et al., 2019). We generated cell lines expressing WT RPL26 or RPL26 containing five lysine
163 to arginine mutations ("5KR RPL26") (Figure 3-figure supplement 3A) and confirmed that ectopic
164 5KR RPL26 was not UFMylated (Figure 3G). HAV infection of WT Huh7.5.1 cells expressing 5KR
165 RPL26 was reduced compared to cells containing ectopic WT RPL26, which largely phenocopied
166 the *UFM1* KO effect (Figure 3H). By contrast, an additional dominant negative effect of 5KR RPL26
167 was not observed in transduced *UFM1* or *UFSP2* KO cells where HAV replication was already
168 lower compared to WT Huh7.5.1 containing WT RPL26 (Figure 3H). Similarly, we measured
169 reduced HAV RNA levels in previously characterized U2OS cells expressing 5KR RPL26 and a
170 CRISPRi system to knockdown endogenous WT RPL26 (Walczak et al., 2019) (Figure 3-figure
171 supplement 3B). Lastly, RV-A2 infection was increased in 5KR RPL26 cells (Figure 3-figure
172 supplement 3C), mirroring the effect of *UFM1* deletion and indicating that UFM1 and RPL26 are
173 functionally linked (Figure 2G). Together, the results support a model that HAV requires active
174 UFMylation of RPL26 for optimal translation.
175

176 PAPD5 and PAPD7 are two non-canonical poly(A) RNA polymerases (ncPAPs), which can transfer
177 oligo(A) to a variety of RNA substrates (including mRNAs, miRNAs, snoRNAs and rRNAs) in a
178 template-independent manner (Berndt et al., 2012; Boele et al., 2014; Rammelt et al., 2011;
179 Shcherbik et al., 2010; Shin et al., 2017). Their activities have been shown to stabilize mRNAs for
180 translation as well as to specify different RNA species for turnover by the exosome complex
181 (Lubas et al., 2011; Vaňáčová et al., 2005; Warkocki et al., 2018). ZCCHC14 has been implicated
182 to interact with these ncPAPs forming a TRAMP-like complex (Go et al., 2019; Hyrina et al., 2019).
183 We measured the effects of either *PAPD5/7* DKO or *ZCCHC14* KO on viral translation and
184 replication using viral replicon RNA and observed a notable defect early post-electroporation
185 before the onset of viral genome replication (Figure 4A). While we detected low levels of
186 replication between 24 and 32h in the host factor KO cell lines, luminescence dropped to near
187 background levels by 48h. We determined that the catalytic activities of PAPD5 and PAPD7 are
188 likely to be required to support viral infection as complementation of KO or DKO cells with WT
189 PAPD5 and/or PAPD7 but not catalytically inactive (CAT) PAPD5 or PAPD7 (containing two
190 aspartate to alanine substitutions in the active site) restored HAV replication (Figure 2-figure
191 supplement 1C and Figure 4-figure supplement 1A-C) (Rammelt et al., 2011). PAPD5 and PAPD7
192 can regulate the length of poly(A) tails of certain mRNAs, which can affect RNA stability and
193 translation (Shin et al., 2017). As HAV has a polyadenylated genome, we assessed the length of
194 viral poly(A) tails from infected WT and DKO cells by polyacrylamide gel electrophoresis but we
195 did not observe a notable difference (Figure 4B). We additionally analyzed the poly(A) tails by
196 TOPO cloning and Sanger sequencing as well as electrophoretic shift using TapeStation with
197 similar results (Figure 4C and Figure 4-figure supplement 2A). By contrast, we observed reduced

198 poly(A) tail lengths as well as infection levels with hepatitis B virus (HBV) in cells deficient of
199 ZCCHC14, a host factor reported to be critical for HBV surface antigen expression (Figure 4-figure
200 supplement 2B and C) (Hyrina et al., 2019).

201 Recently, it was shown that PAPD5 and PAPD7 can introduce guanosines at low
202 frequencies into poly(A) tails resulting in increased stability against CCR4-NOT dependent
203 deadenylation and prolonged mRNA half lives (Lim et al., 2018). However, we did not observe an
204 elevated frequency of non-adenosine nucleotides in WT vs DKO cells within HAV poly(A) tails
205 (Figure 4D and Figure 4-source data 1). Rather, almost all tails exclusively consisted of
206 adenosines. In addition to the absence of changes in HAV poly(A) tail length or composition, we
207 did not detect differences in overall viral RNA levels between WT, DKO as well as *ZCCHC14* KO
208 cells early post viral entry and prior to onset of genome amplification (2-8h) (Figure 4E). Next,
209 using pulse-chase labeling, we did not see a notable difference in HAV RNA decay rates between
210 WT and *PAPD7* KO, which allowed moderate HAV replication but were additionally treated with
211 the PAPD5/7 inhibitor RG7834 prior to the chase to mimic a genetic-chemical DKO condition
212 (Mueller et al., 2019) (Figure 4F).

213 Finally, we probed viral translation directly using the replication-incompetent HAV
214 replicon and observed drastically reduced luciferase levels in the first 10h post-electroporation
215 in DKO and *ZCCHC14* KO cells, consistent with the WT replicon data (Figure 4G). Treatment of WT
216 cells with RG7834 post-electroporation also reduced luminescence levels after 8h (Figure 4-figure
217 supplement 2D). By contrast, translation of electroporated firefly mRNA was not affected and
218 RNA stability as well as poly(A) tail lengths of the *in-vitro* transcribed replicon RNA remained
219 unchanged post-electroporation into DKO cells (Figure 4-figure supplement 2E and F). Therefore,

220 we propose a critical role of the TRAMP-like complex in facilitating HAV translation in a HAV
221 poly(A) tail length and RNA stability-independent manner.
222
223 Next, we sought to explore whether pharmacological inhibition of PAPD5/7 exhibits an antiviral
224 effect on HAV replication. We used RG7834 (Figure 5A), a small molecule compound belonging
225 to the chemical class of the dihydroquinolizinones, which was first identified as a potent inhibitor
226 for HBV surface antigen secretion (Mueller et al., 2018). Additional studies using yeast three-
227 hybrid screening identified PAPD5 and PAPD7 as the cellular targets for RG7834 (Mueller et al.,
228 2019). We performed a dose-response curve and calculated a 50% effective concentration (EC_{50})
229 of 12.76nM for inhibition of HAV replication, which is far below the reported 50% cytotoxic
230 concentration (CC_{50}) of >10 µM and consistent with our measurements (Figure 5B and Figure 5-
231 figure supplement 1A) (Mueller et al., 2018). Drug treatment of infected *PAPD5* or *PAPD7* KO
232 cells suggested that RG7834 has a stronger inhibitory effect on the PAPD5 activity as reduction
233 of viral RNA is more substantial in the *PAPD7* KO+RG7834 condition (Figure 5-figure supplement
234 1B). Intrigued by the fact that RG7834 inhibits both HAV and HBV, we also measured the effects
235 on two additional liver-specific viruses, HCV and hepatitis E virus (HEV). However, RG7834 only
236 showed significant reduction of HAV and HBV RNA levels (Figure 5C-F). This is consistent with
237 unchanged viral replication levels of HCV and HEV in DKO cells (Figure 5-figure supplement 1C).
238 Finally, we performed infection assays in human liver organoid cultures (Broutier et al., 2016).
239 We observed significant reduction of HAV RNA in both stem cell-like and differentiated organoids
240 under RG7834 treatment (Figure 5G and Figure 5-figure supplement 1D), highlighting that

241 pharmacological targeting of PAPD5/7 is a promising strategy for host-directed therapy of HAV
242 infection.
243
244 **Discussion**
245 This study provides a comprehensive assessment of the host factors that are required for HAV
246 infection. We revealed two cellular pathways, UFMylation and a TRAMP-like complex, which had
247 not been implicated in HAV life cycle before. We demonstrated that UFMylation is required for
248 optimal HAV translation in an RPL26-UFM1-conjugation dependent manner. The cellular function
249 of this protein modification is still an emerging field of research but it has been linked to the
250 regulation of the ER stress response and ribosome-associated quality control (Walczak et al.,
251 2019; Wang et al., 2019). Specific ribosomal or ribosome-associated proteins have been shown
252 to be required for efficient translation of viral genomes (Landry et al., 2009; Majzoub et al., 2014).
253 RPL26 is located near the ribosome exit tunnel and its modification could facilitate dynamic and
254 reversible conformation changes to improve translation of specific amino acid sequences or
255 resolve certain secondary structure in the RNA as suggested by the requirement for active
256 UFMylation and de-UFMylation during HAV infection. Additional studies, such as biochemical
257 analysis and ribosome profiling of the different ribosomal subpopulations, are needed to gain a
258 better understanding of its role during translation of viral and cellular mRNAs. The contrasting
259 phenotypes observed during HAV and RV-A2 infection in *UFM1* KO cells may also be utilized as
260 tools for future studies of the molecular effects of UFMylation.
261 Furthermore, we identified the TRAMP-like complex components ZCCHC14, PAPD5 and
262 PAPD7. In the context of the nuclear TRAMP machinery, PAPD5/7 interact with ZCCHC7, another

263 CCHC-motif containing zinc knuckle protein, and the Mtr4 exosome RNA helicase
264 (MTREX/SKIV2L2) (Lubas et al., 2011), which were not enriched in the HAV CRISPR screen. This
265 suggests that PAPD5/7 can form different complexes with specific cellular activities. For example,
266 template-independent polyadenylation of nuclear RNA substrates with short oligo(A) tails for
267 targeted degradation by the exosome as well as increase of mRNA stability by poly(A) tail
268 extension or mixed tailing have been reported (Schmid and Jensen, 2018; Warkocki et al., 2018).
269 We revealed that the pro-viral function of the TRAMP-like complex is important for the
270 translatability of HAV RNA, independent from modifying its poly(A) tails. This is consistent with
271 previous observations that picornavirus polyadenylation is template-dependent, for example by
272 the presence of a homotypic poly(U) sequence in the picornavirus negative-sense RNA (Spector
273 and Baltimore, 1975). Moreover, studies using poliovirus, another picornavirus, suggested that
274 the picornaviral RNA-dependent RNA polymerase uses reiterative transcription as it replicates
275 the poly(A) tails of viral RNA (Kempf et al., 2013; Steil et al., 2010). These findings support that
276 ncPAPs are not required for HAV poly(A) tail generation or maintenance. In studies using *C.*
277 *elegans*, deletion of the worm orthologs of PAPD5 (gld-4) and ZCCHC14 (gls-1) led to reduced
278 polysome formation but did not affect global poly(A) tail lengths, providing evidence of
279 polyadenylation-independent functions of TRAMP-like complexes (Nousch et al., 2014).
280 Unexpectedly, we found that mutations in the active sites of PAPD5/7 affected HAV infection. It
281 is possible that the catalytic mutations have structural implications and impair the co-opted non-
282 catalytic activity or, alternatively, PAPD5 and PAPD7 regulate another host factor critical to HAV
283 translation through RNA tailing.

284 Interestingly, other tested picornaviruses were not dependent on the TRAMP-like
285 complex for efficient translation despite commonalities in their gene expression strategy.
286 Surprisingly though, PAPD5, PAPD7 and ZCCHC14 were identified as critical factors for infection
287 with HBV, a hepatotropic DNA virus with a vastly different life cycle, using chemical and CRISPR
288 screens (Hyrina et al., 2019; Mueller et al., 2019). Mechanistically, the TRAMP-like complex plays
289 an important role in HBsAg expression by poly(A) tail extension of HBsAg mRNAs (Hyrina et al.,
290 2019). This highlights a remarkable convergence of two unrelated hepatitis viruses to co-opt the
291 same cellular complex. Finally, we provided proof-of-concept that pharmacological inhibition of
292 PAPD5 and PAPD7 decreases HAV as well as HBV levels. Overall, this study provides a
293 comprehensive picture of HAV host factors and uncovered UFMylation and the TRAMP-like
294 complex as important components for successful viral protein biogenesis.

Figure 1

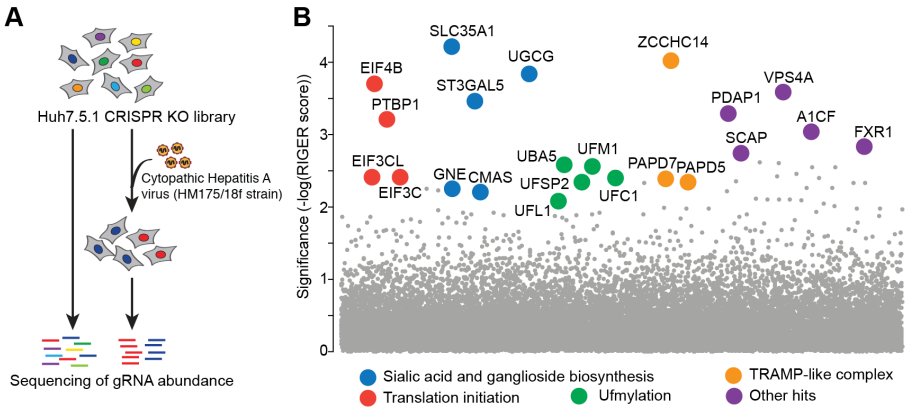

C

GO term	p-value
protein K69-linked ufmylation	9.20E-10
mitochondrial RNA catabolic process	5.09E-07
RNA polyadenylation	4.70E-06
ubiquinone biosynthetic process	2.77E-05
translation initiation factor activity	3.73E-05
TRAMP complex	8.35E-05
Ragulator complex	2.08E-04
N-acetylneuraminate metabolic process	7.53E-04

Figure 1. Genome-wide CRISPR KO screen identifies host cellular factors important for HAV infection. (A) Schematic of the genome-wide CRISPR KO screening setup. A library of Huh7.5.1 CRISPR-Cas9 cells was infected with cytopathic HAV HM175/18f and virus-resistant cells were harvested 12 days post-infection (dpi). gRNA abundance was measured in the original and selected cell population by next-generation sequencing. **(B)** RIGER analysis to calculate the significance of enriched genes in CRISPR KO screen. Enriched genes were clustered and colored by function. The screen was performed once. **(C)** Selected terms from gene ontology (GO) analysis of genes enriched in CRISPR KO screen (RIGER p-value < 0.001).

Figure 1 - figure supplement 1

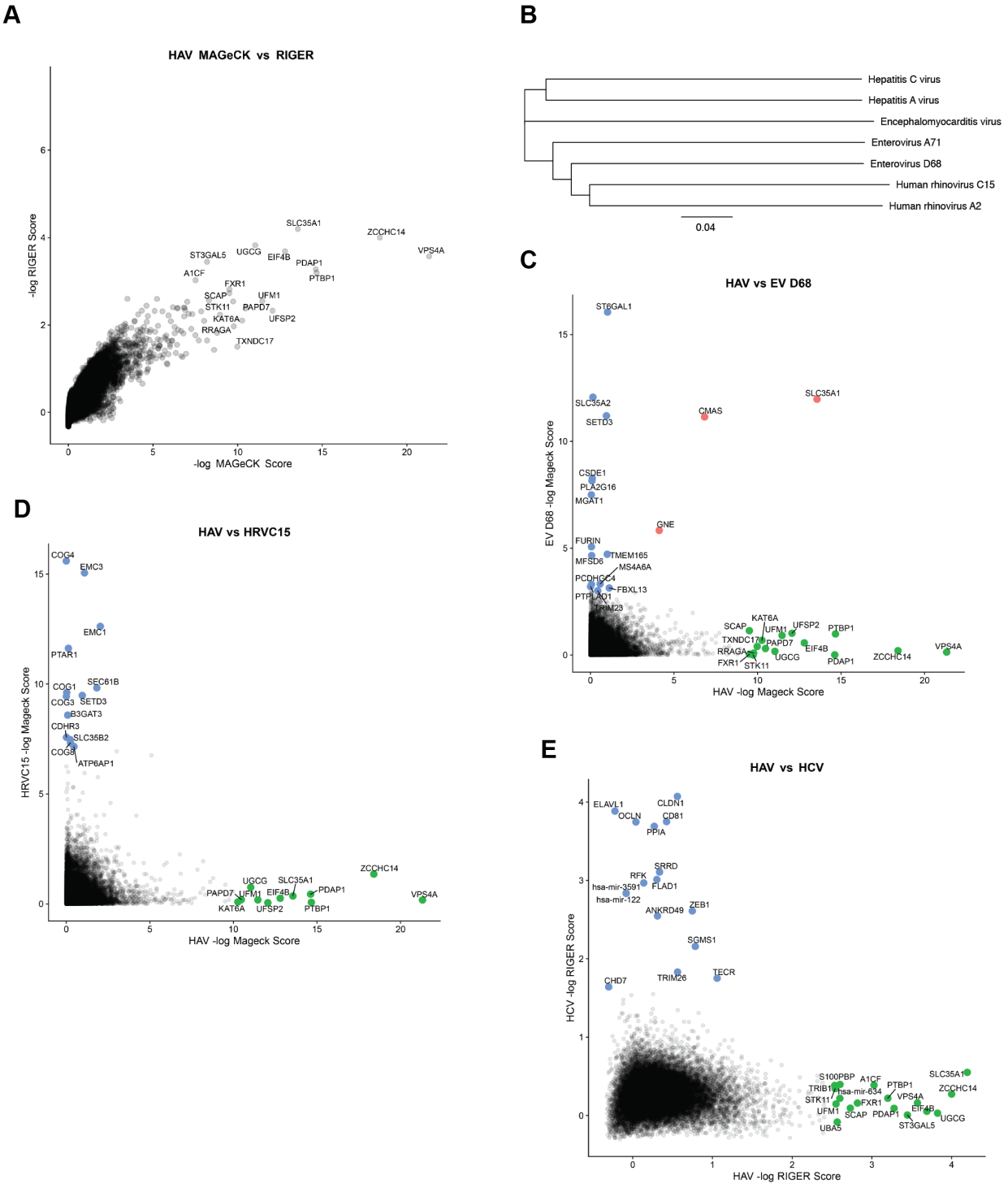

306

307 **Figure 1-figure supplement 1. Comparative analysis of CRISPR screen results for HAV,**

308 **enterovirus D68, rhinovirus C15 and HCV host factors. (A)** Comparison of RIGER and MaGECK

309 analysis of HAV CRISPR screen. **(B)** Phylogenetic tree of HAV, HCV, EMCV, enterovirus A71,
310 enterovirus D68, rhinovirus A2 and rhinovirus C15. **(C)** Comparison of HAV CRISPR screen results
311 from this study with enterovirus D68 CRISPR screen results from (Diep et al., 2019) using MaGECK
312 analysis. **(D)** Comparison of HAV CRISPR screen results from this study with human rhinovirus C15
313 CRISPR screen results from (Diep et al., 2019) using MaGECK analysis. **(E)** Comparison of HAV
314 CRISPR screen results from this study with HCV CRISPR screen results from (Marceau et al., 2016)
315 using RIGER analysis.

Figure 2

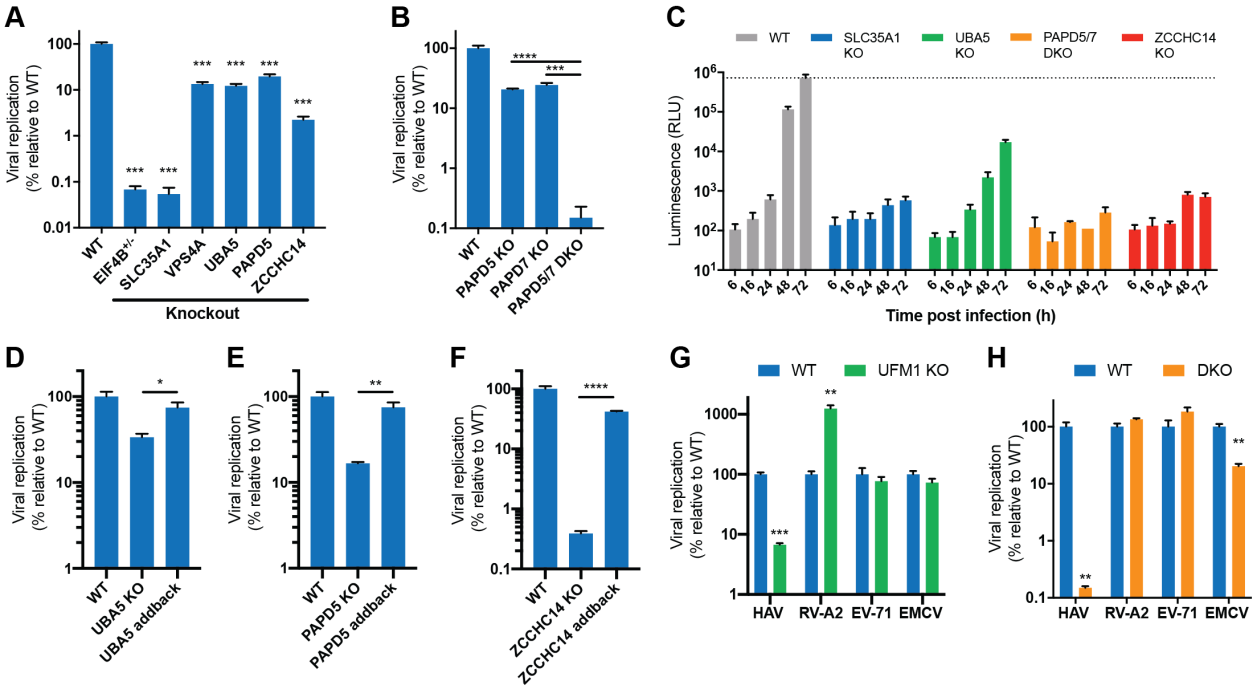

Figure 2. Validation of identified HAV host factors. (A) Quantification of HAV RNA in WT and clonal KO cell lines 3 dpi by RT-qPCR. **(B)** Quantification of HAV RNA in WT, *PAPD5* KO, *PAPD7* KO and *PAPD5/PAPD7* double KO (DKO) cells 3 dpi by RT-qPCR. **(C)** Viral growth curves using recombinant HAV expressing nanoluciferase (HAV-Nluc). WT, *SLC35A1* KO, *UBA5* KO, *PAPD5/7* DKO and *ZCCHC14* KO cells were infected, lysed at indicated timepoints and luciferase levels were measured. Dotted line indicates luminescence levels in WT cells at 72 hpi. Data are displayed as means ± s.d. (n=2 biological replicates). **(D-F)** Quantification of HAV RNA in WT, *UBA5* KO (**D**), *PAPD5* KO (**E**), or *ZCCHC14* KO (**F**) cells and KO cells complemented with respective cDNAs 3 dpi by RT-qPCR. **(G-H)** Quantification of HAV, human rhinovirus A2 (RV-A2), enterovirus 71 (EV-71) and encephalomyocarditis virus (EMCV) RNA in WT vs *UFM1* KO cells (**G**) or WT vs DKO cells (**H**) by RT-qPCR. Cells infected with HAV or RV-A2 were harvested after 48h, with EV-71 after 24h and with EMCV after 8h.

329 For all RT-qPCR experiments, viral RNA was normalized to 18S RNA and results are displayed
330 relative to infection in WT cells. Datasets represent means ± s.e.m. (n=3 biological replicates). P
331 values were determined by unpaired two-sided t-tests using GraphPad Prism 8. *, $p<0.05$; **,
332 $p<0.01$; ***, $p<0.001$; ****<0.0001.

Figure 2 - figure supplement 1

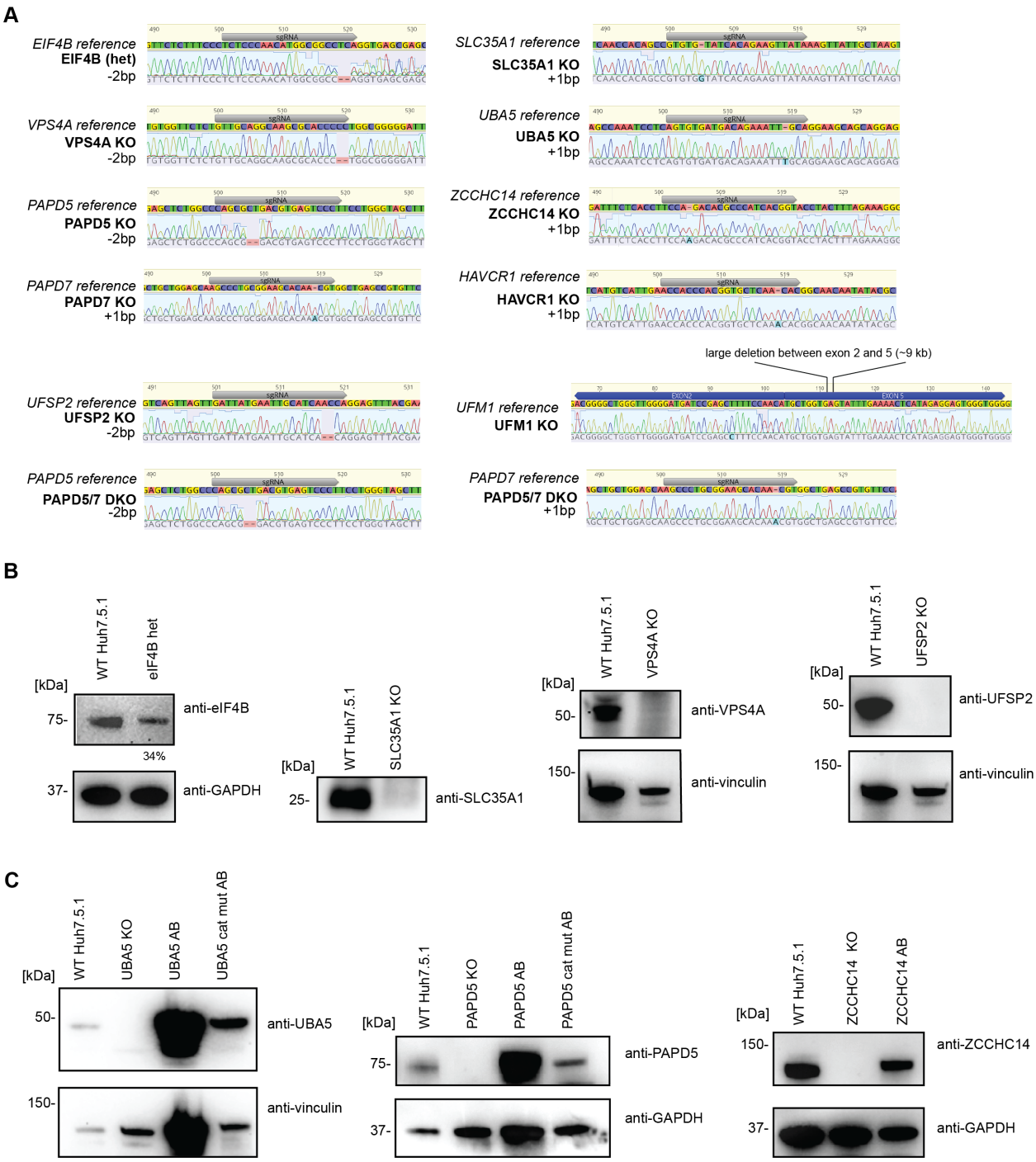

Figure 2-figure supplement 1. Genotyping and immunoblotting of clonal Huh7.5.1 KO cell lines. **(A)** Sanger sequencing of gRNA targeted loci of clonal KO cell lines. Traces were aligned to corresponding reference sequences and indel mutations determined. Reads of gRNA targeted

337 PAPD5 and PAPD7 loci in clonal Huh7.5.1 DKO cells are displayed. UFM1 gene was simultaneously
338 targeted by two gRNAs cutting in exon 2 and exon 5 resulting in a large genomic deletion. **(B)**
339 Immunoblots for clonal *eIF4B*, *SLC35A1*, *VPS4A* and *UFSP2* KO cell lines. For eIF4B, a heterozygous
340 clone harboring one allele with a -2bp deletion and one WT allele, quantification of the band (in
341 %) is normalized to GAPDH signal and relative to WT indicating decrease of expression in
342 heterozygous clone. For SLC35A1, WT and KO cells were lysed in RIPA buffer and lysates were
343 immunoprecipitated using anti-SLC35A1 antibody and protein G beads prior to immunoblot.
344 GAPDH and Vinculin were used as loading controls. **(C)** Immunoblots of WT, *UBA5* KO, *PAPD5* KO
345 or *ZCCHC14* KO cells as well as KO cells complemented with respective cDNAs. GAPDH and
346 Vinculin were used as loading controls.

Figure 2 - figure supplement 2

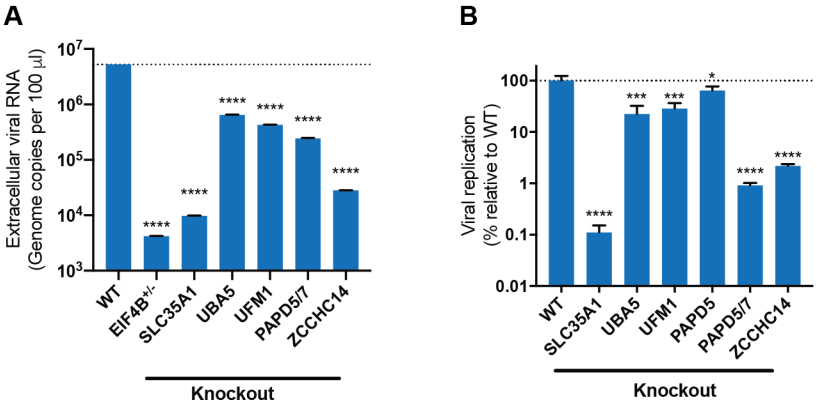

Figure 2-figure supplement 2. Measurement of extracellular viral RNA and validation of HAV host factors using a lower-passage HAV HM175 strain. (A) Quantification of extracellular viral RNA in supernatant of cells 3 dpi using HM175/18f HAV. RNA was extracted from supernatant, measured by RT-qPCR and compared to a standard curve of in vitro transcribed viral RNA to determine genome copies. Dataset represents means ± s.e.m. (n=2 biological replicates). **(B)** Quantification of HAV RNA in WT or clonal KO cell lines by RT-qPCR using a lower passage HAV strain. Viral RNA was normalized to 18S RNA and results are displayed relative to infection in WT cells. Dataset represents means ± s.e.m. (n=3 biological replicates).

P values were determined by one-way Anova with uncorrected Fisher's Least Significant Difference test using GraphPad Prism 8. *, $p<0.05$; **, $p<0.01$; ***, $p<0.001$; ****<0.0001.

Figure 2 - figure supplement 3

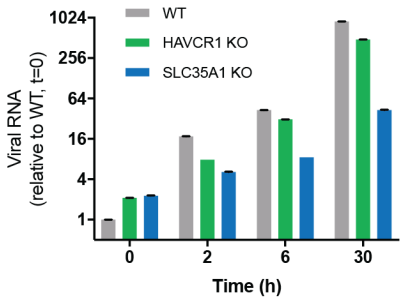

358

359 **Figure 2-figure supplement 3. Viral attachment and entry assay.** Quantification of HAV RNA in

360 WT, *HAVCR1* KO and *SLC35A1* KO cells by RT-qPCR after cells were infected on ice, incubated at

361 37C, and washed before harvest at indicated times. Viral RNA was normalized to 18S RNA and

362 results are displayed relative to infection in WT cells. Datasets represent means ± s.e.m. (n=3

363 biological replicates).

364

Figure 3

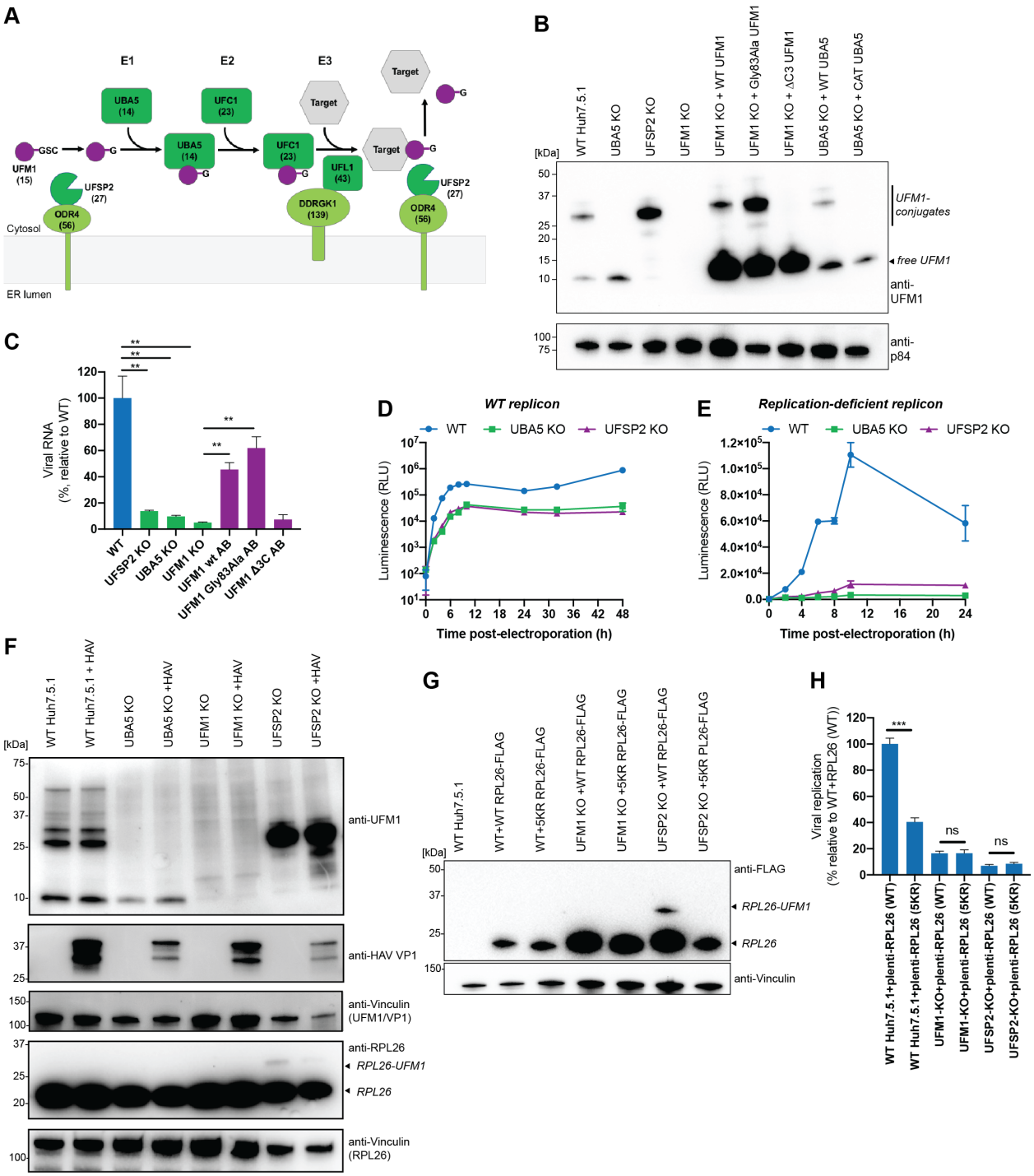

Figure 3. HAV depends on functional UFM1 conjugation of the ribosomal protein RPL26 for optimal translation. (A) Schematic of cellular UFMylation pathway. (#) indicates rank of gene in the RIGER analysis of CRISPR screen. **(B)** UFM1 immunoblot of WT, *UFSP2* KO, *UBA5* KO, *UFM1*

369 KO and *UFM1* KO cells complemented with WT, Gly83Ala or ΔC3 UFM1 as well as *UBA5* KO cells
370 complemented with WT or catalytically inactive UBA5. Upper bands represent UFM1 conjugation
371 products and bottom band represents free UFM1. P84 was used as loading control. **(C)**
372 Quantification of HAV RNA in WT, *UFSP2* KO, *UBA5* KO, *UFM1* KO and *UFM1* KO cells
373 complemented with WT, Gly83Ala or ΔC3 UFM1. Viral RNA was normalized to 18S RNA and
374 results are displayed relative to infection in WT cells. **(D)** Timecourse of luciferase activity
375 expressed by electroporated HAV-FLuc subgenomic replicon RNA in WT, *UBA5* KO and *UFSP2* KO
376 cells. **(E)** Timecourse of luciferase activity expressed by electroporated HAV-FLuc replication-
377 incompetent replicon RNA in WT, *UBA5* KO and *UFSP2* KO cells. **(F)** Immunoblots of uninfected
378 and HAV infected WT, *UBA5* KO, *UFM1* KO and *UFSP2* KO cells. Membranes were stained with
379 anti-UFM1, anti-HAV VP1 or anti-RPL26 antibodies. Anti-Vinculin served as loading control. **(G)**
380 FLAG immunoblot of WT, *UFM1* KO and *UFSP2* KO cells transduced with lentivirus expressing
381 FLAG-tagged WT RPL26 or 5KR RPL26. Vinculin served as loading control. **(H)** Quantification of
382 HAV RNA in WT, *UFM1* KO and *UFSP2* KO cells transduced with lentivirus expressing FLAG-tagged
383 WT RPL26 or RPL26 containing five lysine to arginine (5KR) mutations in the UFM1 acceptor site.
384 Viral RNA was normalized to 18S RNA and results are displayed relative to infection in WT cells
385 expressing WT RPL26.
386 For all RT-qPCR experiments, datasets represent means ± s.e.m. (n=3 biological replicates). For
387 luciferase experiments, datasets represent means ± s.d. (n=2 biological replicates) for each
388 timepoint. P values were determined by unpaired two-sided t-tests using GraphPad Prism 8. ns,
389 non-significant; *, $p<0.05$; **, $p<0.01$; ***, $p<0.001$; ****<0.0001.

Figure 3 - figure supplement 1

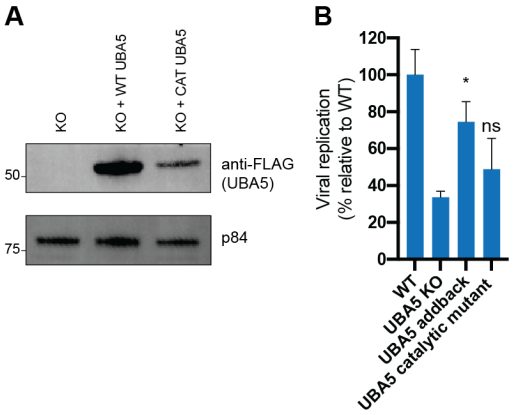

Figure 3-figure supplement 1. HAV depends on catalytically active UBA5. (A) FLAG immunoblot of lysates from *UBA5* KO cells transduced with FLAG-tagged WT or catalytically inactive (CAT) UBA5. P84 was used as loading control. **(B)** Quantification of HAV RNA in WT, *UBA5* KO and *UBA5* KO complemented with WT or CAT UBA5 3 dpi by RT-qPCR. Viral RNA was normalized to 18S RNA and results are displayed relative to infection in WT cells. Datasets represent means ± s.e.m. (n=3 biological replicates). P values were determined by unpaired two-sided t-tests using GraphPad Prism 8. ns, non-significant; *, $p<0.05$.

Figure 3 - figure supplement 2

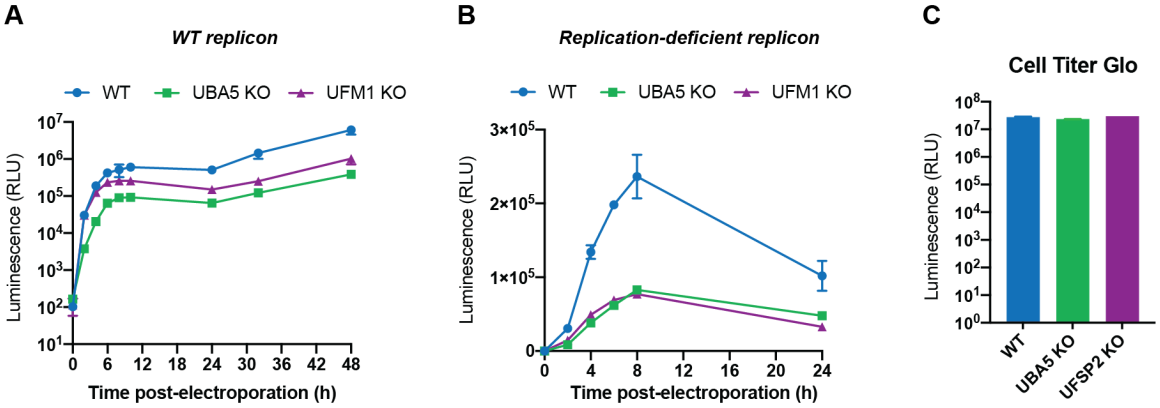

Figure 3-figure supplement 2. HAV translation is impaired in UFMylation deficient cells. (A) Timecourse of luciferase activity expressed by electroporated HAV-FLuc subgenomic replicon RNA in WT, *UBA5* KO and *UFM1* KO cells. Datasets represent means ± s.d. (n=2 biological replicates) for each timepoint. **(B)** Timecourse of luciferase activity expressed by electroporated HAV-FLuc replication-incompetent replicon RNA in WT, *UBA5* KO and *UFM1* KO cells. Datasets represent means ± s.d. (n=2 biological replicates) for each timepoint. **(C)** Cell Titer Glo assay to measure cell viability of electroporated WT, *UBA5* KO and *UFSP2* KO cells 24h post-electroporation. Datasets represent means ± s.d. (n=2 biological replicates).

Figure 3 - figure supplement 3

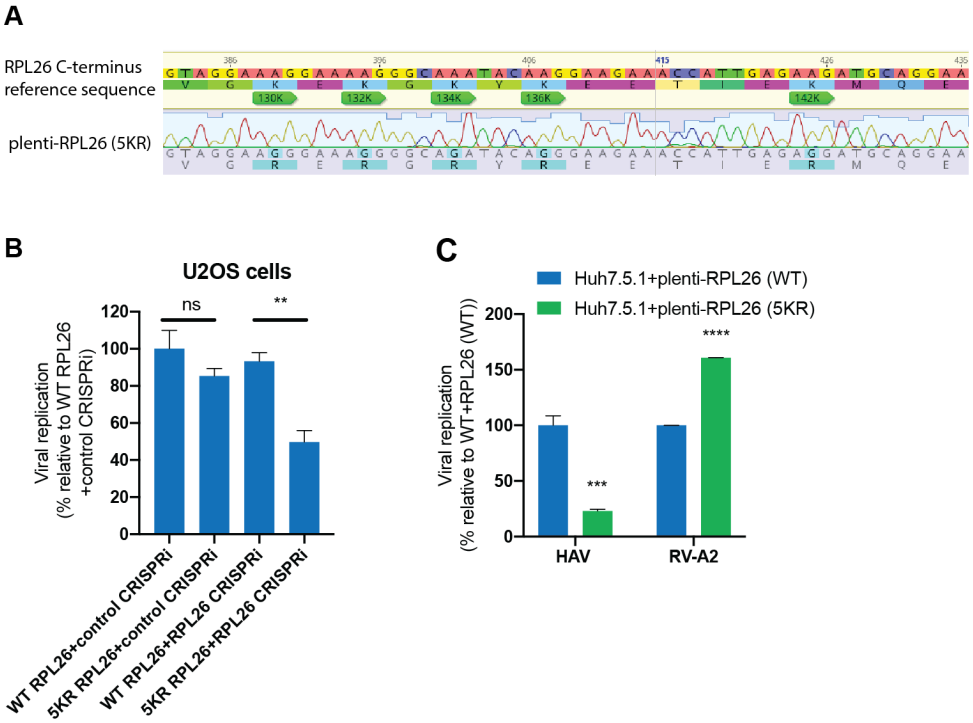

Figure 3-figure supplement 3. UFM1 conjugation to C-terminal lysines of RPL26 is required for optimal HAV infection. (A) Reference and Sanger sequence of lentiviral construct expressing RPL26 with five lysine to arginine point mutations at C-terminus (5KR). **(B)** Quantification of HAV RNA in U2OS dCas9-KRAB cells expressing WT RPL26 or 5KR RPL26 as well as a control (non-targeting) or RPL26 targeting gRNA. Viral RNA was normalized to 18S RNA and results are displayed relative to infection in cells expressing WT RPL26 and the control gRNA. **(C)** Quantification of HAV and RV-A2 RNA in WT cells transduced with lentivirus expressing FLAG-tagged WT RPL26 or 5KR RPL26. Viral RNA was normalized to 18S RNA and results are displayed relative to infection in WT cells expressing WT RPL26.

419 Dataset represents means ± s.e.m. (n=3 biological replicates). P values were determined by

420 unpaired two-sided t-tests using GraphPad Prism 8. ns, non-significant; *, $p<0.05$; **, $p<0.01$;

421 ***, $p<0.001$; ****<0.0001.

422

Figure 4

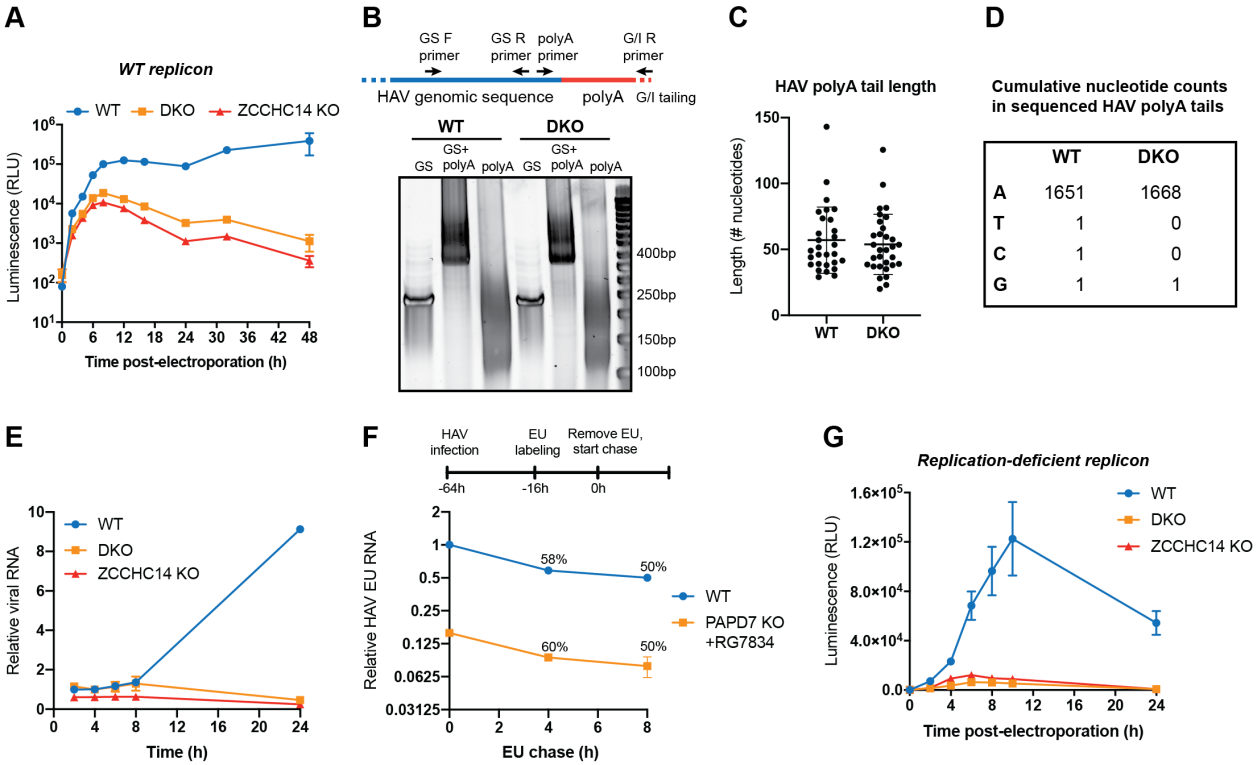

Figure 4. TRAMP-like complex is important for HAV translation independent of viral poly(A) tail length or RNA stability. (A) Timecourse of luciferase activity expressed by electroporated HAV-FLuc subgenomic replicon RNA in WT, DKO and *ZCCHC14* KO cells. Datasets represent means ± s.d. (n=2 biological replicates) for each timepoint. **(B)** HAV poly(A) tail length assay. Total RNA from infected WT or DKO cells was G/I tailed at 3'ends, reverse transcribed and PCR amplified by i) HAV genome-specific (GS) forward and GS reverse primer, ii) GS forward and G/I reverse primer and iii) forward primer upstream of HAV poly(A) start site and G/I reverse primer. PCR products were analyzed by polyacrylamide gel electrophoresis. **(C)** Length distribution of sequenced HAV poly(A) tails. An RNA linker was ligated to 3'ends of rRNA-depleted RNA from infected WT or DKO cells followed by reverse transcription and PCR amplification of the HAV poly(A) tail region. PCR products were TOPO cloned and Sanger sequenced. **(D)** Analysis of nucleotide composition of

435 sequenced HAV poly(A) tails from (C). **(E)** Quantification of HAV RNA in WT, DKO and *ZCCHC14*
436 KO cells by RT-qPCR after cells were infected on ice and incubated at 37C for 1h. Subsequently
437 cells were washed 3 times and bound virus stripped away by trypsinization to prevent any further
438 viral uptake. Finally, cells were harvested at indicated times. Viral RNA was normalized to 18S
439 RNA. Datasets represent means ± s.e.m. (n=3 biological replicates). **(F)** Ethynyl uridine (EU) pulse-
440 chase experiment to measure viral RNA decay. WT and partially permissive *PAPD7* KO cells were
441 infected for 64h to allow sufficient viral RNA accumulation. EU was added for 16h. Additionally,
442 the PAPD5/7 inhibitor RG7834 was added to *PAPD7* KO to block remaining PAPD5 activity. At
443 t=0h EU was removed and total RNA was harvested at indicated timepoints. EU labeled RNA was
444 isolated by biotin click chemistry and quantified using RT-qPCR. Viral EU RNA was normalized to
445 18S RNA. Datasets represent means ± s.e.m. (n=2 biological replicates). Percentages indicate RNA
446 levels relative to respective t=0h levels in WT and *PAPD7* KO cells. **(G)** Timecourse of luciferase
447 activity expressed by electroporated HAV-FLuc replication-incompetent replicon RNA in WT, DKO
448 cells and *ZCCHC14* KO. Datasets represent means ± s.d. (n=2 biological replicates) for each
449 timepoint.
450

Figure 4 - figure supplement 1

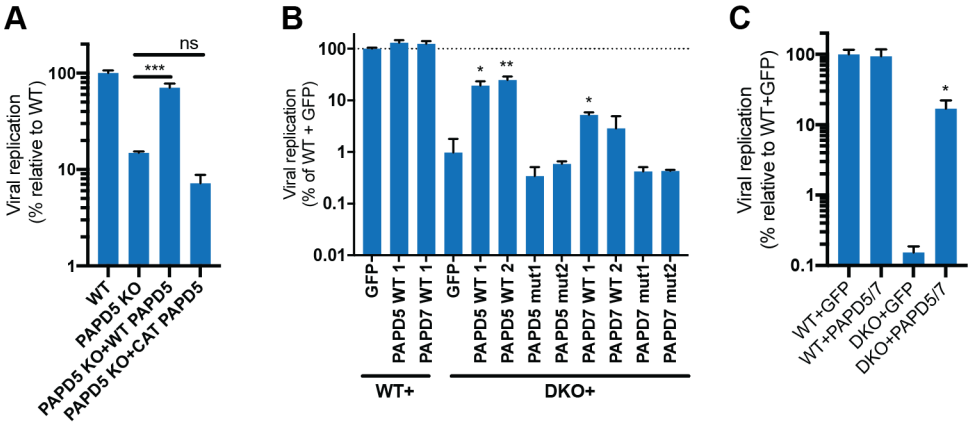

Figure 4-figure supplement 1. Catalytic activities of PAPD5 and PAPD7 are required for HAV infection. (A) Quantification of HAV RNA in WT, *PAPD5* KO and *PAPD5* KO cells complemented with either WT or catalytically inactive (CAT) PAPD5 3 dpi by RT-qPCR. Viral RNA was normalized to 18S RNA and results are displayed relative to infection in WT cells. Datasets represent means ± s.e.m. (n=3 biological replicates). **(B)** Quantification of HAV RNA in DKO cells transfected with GFP cDNA, PAPD5 WT or CAT cDNA, or PAPD7 WT or CAT cDNA 3 dpi by RT-qPCR. Viral RNA was normalized to 18S RNA and results are displayed relative to infection in WT cells transfected with GFP cDNA. Datasets represent means ± s.e.m. (n=3 biological replicates). **(C)** Quantification of HAV RNA in WT or DKO cells transfected with GFP cDNA or co-transfected with both PAPD5 and PAPD7 WT cDNAs. Datasets represent means ± s.e.m. (n=3 biological replicates).

P values were determined by unpaired two-sided t-tests using GraphPad Prism 8. ns, non-significant; *, $p<0.05$; **, $p<0.01$; ***, $p<0.001$.

Figure 4 - figure supplement 2

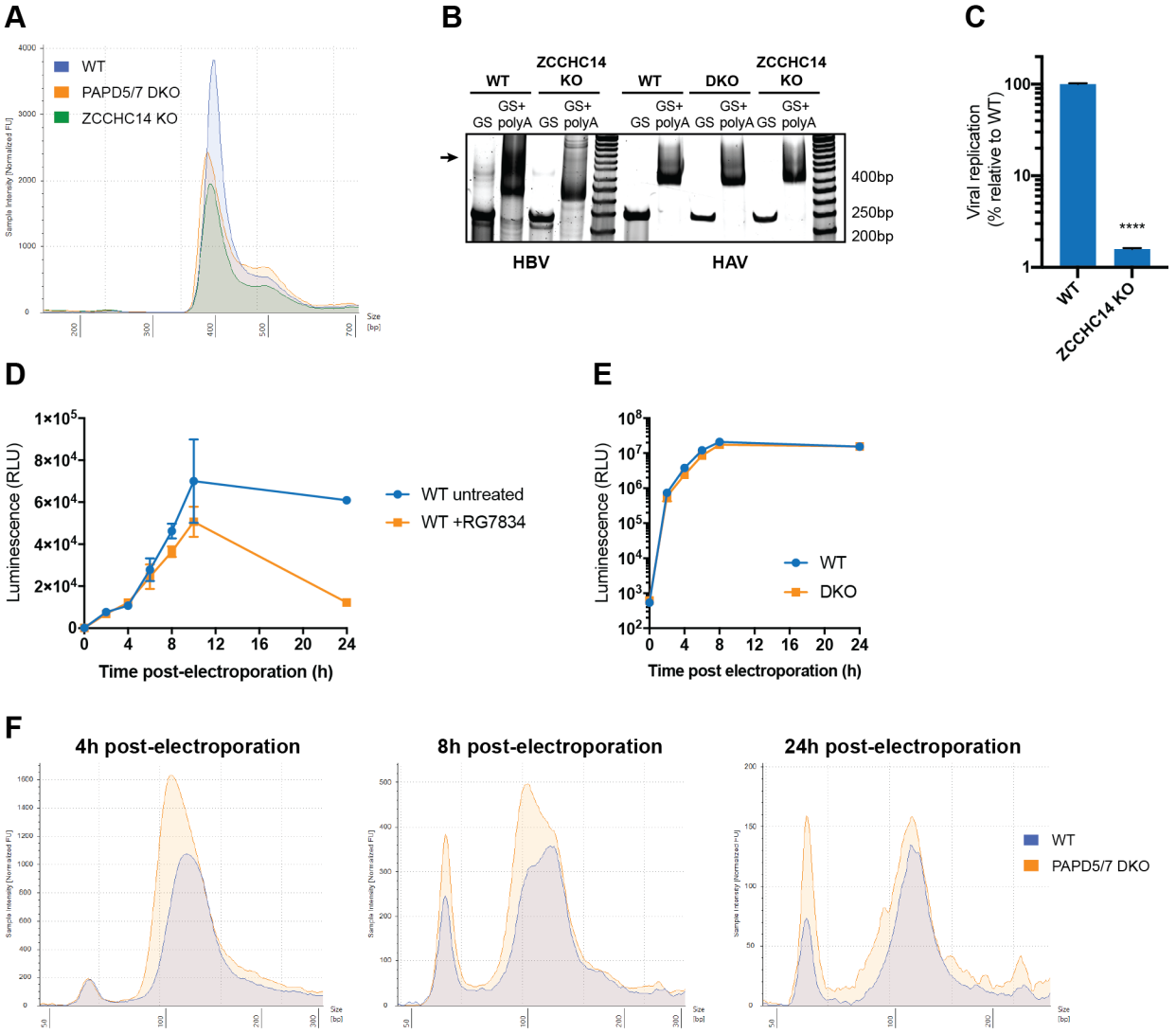

Figure 4-figure supplement 2. TRAMP-like complex supports HAV translation independent of viral RNA stabilization. (A) Electrophoretic analysis of poly(A) tail region of HAV from infected WT, DKO and *ZCCHC14* KO cells at 72hpi. Total RNA was G/I tailed at 3'ends, reverse transcribed and PCR amplified by forward primer ~300bp upstream of HAV poly(A) start site and G/I reverse primer. **(B)** Polyacrylamide gel analysis of amplified HBV poly(A) tail region from infected WT or *ZCCHC14* KO HepG2-NTCP cells as well as of amplified HAV poly(A) tail region from infected WT, DKO and *ZCCHC14* KO Huh7.5.1 cells. Arrow indicates a longer HBV poly(A) tail in WT cells. **(C)**

473 Quantification of HBV RNA in WT and *ZCCHC14* KO HepG2-NTCP cells 14dpi. Viral RNA was
474 normalized to 18S RNA and results are displayed relative to infection in WT cells. Datasets
475 represent means ± s.e.m. (n=3 biological replicates). **(D)** Timecourse of luciferase activity
476 expressed by electroporated HAV-FLuc replication-incompetent replicon RNA in WT cells, left
477 untreated or treated with RG7834 post-electroporation. Datasets represent means ± s.d. (n=2
478 biological replicates) for each timepoint. **(E)** Timecourse of luciferase activity expressed by
479 electroporated firefly mRNA in WT and DKO cells. Datasets represent the means ± s.d. (n=2
480 biological replicates). **(F)** Electrophoretic analysis of poly(A) tail region of electroporated HAV
481 replicon RNA in WT and DKO cells at 4, 8 and 24h post-electroporation. Total RNA from
482 electroporated cells was G/I tailed at 3'ends, reverse transcribed and PCR amplified by forward
483 primer near HAV poly(A) start site and G/I reverse primer. Expected product size for full-length
484 *in-vitro* transcribed (IVT) RNA is 124bp (containing a 40bp poly(A) tail).
485 P values were determined by unpaired two-sided t-tests using GraphPad Prism 8. ****, $p<0.0001$.
486

Figure 5

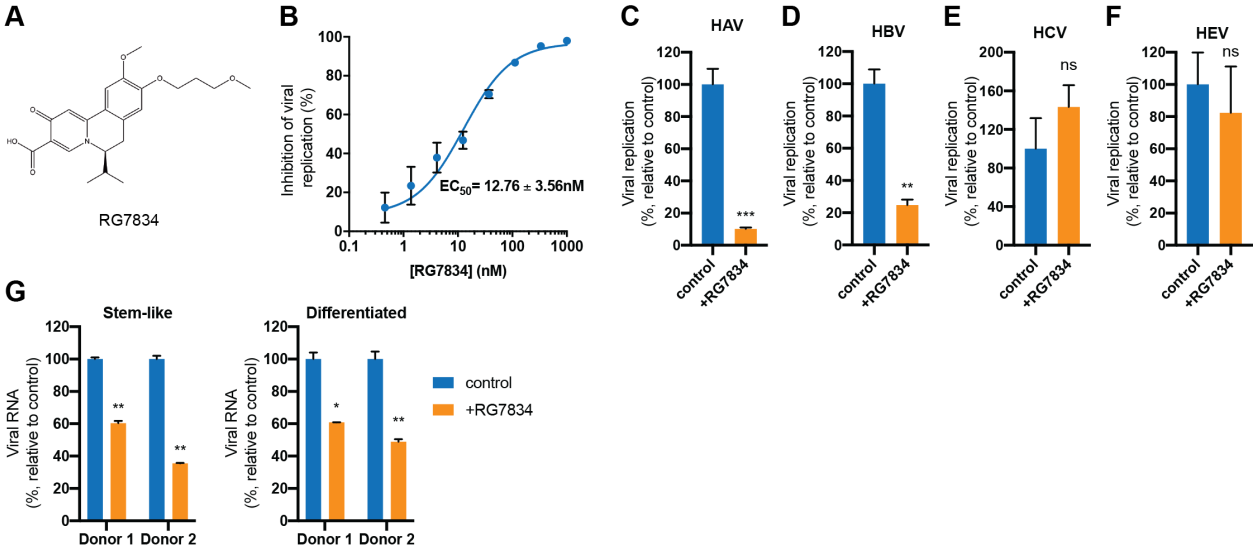

Figure 5. Small molecule inhibition of PAPD5 and PAPD7 reduces HAV infection in human hepatocyte cells and human liver organoids. (A) Chemical structure of RG7834. **(B)** Dose-response curve of HAV RNA levels in Huh7.5.1 cells treated with different RG7834 concentrations as measured by RT-qPCR 3 days post-infection/treatment. Non-linear curve was fitted with least squares regression using GraphPad Prism 8 and EC_{50} was determined. **(C)** Quantification of HAV RNA in control and RG7834 (100 nM) treated Huh7.5.1 cells 3 dpi by RT-qPCR. **(D)** Quantification of HBV total RNA in control and RG7834 (100 nM) treated HepG2-NTCP cells 15 dpi by RT-qPCR. Drug was replenished every 3-4 days. **(E)** Quantification of HCV RNA in control and RG7834 (100 nM) treated Huh7.5.1 cells 3 dpi by RT-qPCR. **(F)** Quantification of HEV RNA in control and RG7834 (100 nM) treated Huh7.5.1 cells by RT-qPCR 6 days post-transfection of viral RNA. **(G)** Quantification of HAV RNA in control and RG7834 (100 nM) treated human liver organoids 7 dpi by RT-qPCR. Organoids were either stem-like or differentiated to adult hepatocytes prior to infection.

501 For all RT-qPCR experiments, viral RNA was normalized to 18S RNA and results are displayed
502 relative to infection in control (DMSO) condition. Datasets in (**B-F**) represent means ± s.e.m. (n=3
503 biological replicates). For organoid experiments (**G**) donor 1 and 2 represent 2 independent
504 biological replicates and qPCR was performed with 2 technical replicates. P values were
505 determined by unpaired two-sided t-tests using GraphPad Prism 8. ns, non-significant; *, $p<0.05$;
506 **, $p<0.01$; ***, $p<0.001$.

Figure 5 - figure supplement 1

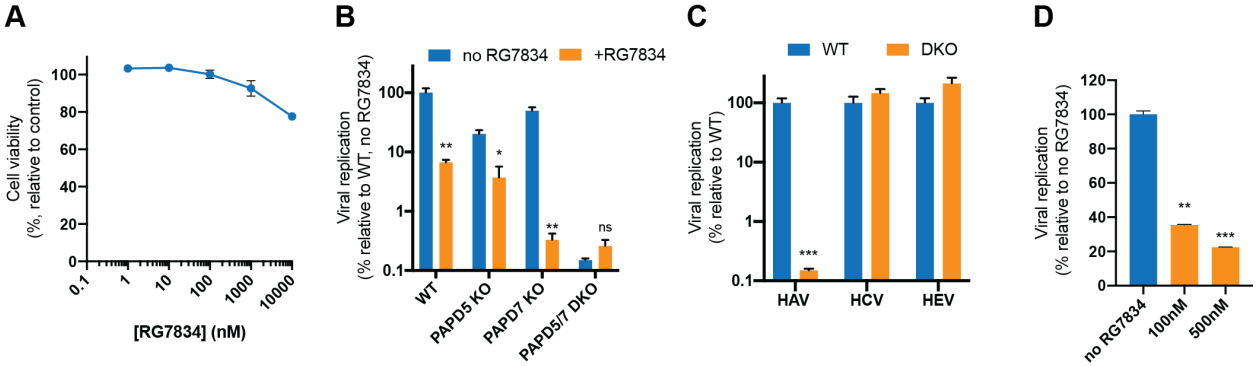

507

508 **Figure 5-figure supplement 1. Small molecule inhibition of PAPD5 and PAPD7 reduces HAV**

509 **infection in human hepatocyte cells and human liver organoids. (A)** Cell viability assay of

510 Huh7.5.1 cells treated with different concentrations of RG7834 for 3 days. Dataset represents

511 means ± s.d. (n=3 biological replicates) for each time point and values are relative to DMSO

512 treated control. **(B)** Quantification of HAV RNA in WT, *PAPD5* KO, *PAPD7* KO or DKO cells

513 untreated or treated with 100 nM RG7834 3 dpi by RT-qPCR. **(C)** Quantification of HAV and HCV

514 RNA 3 dpi, and of HEV RNA 5 days post viral RNA transfection in WT or DKO cells using RT-qPCR.

515 **(D)** Quantification of HAV RNA in human liver organoids treated with no, 100 nM or 500 nM

516 RG7834 by RT-qPCR.

517 For RT-qPCR experiments, viral RNA was normalized to 18S RNA and results are displayed relative

518 to infection in (untreated) WT cells. Datasets represent means ± s.e.m. (n=3 biological replicates).

519 P values were determined by unpaired two-sided t-tests using GraphPad Prism 8. ns, non-

520 significant; *, p<0.05; **, p<0.01; ***, p<0.001; ****<0.0001.

521

522 **Methods**

523 Cell lines, viruses and reagents

524 Huh7.5.1 (gift from Frank Chisari), HEK293FT (Thermo Scientific) and U2OS cells (gift from Ron
525 Kopito) were cultured in DMEM (Gibco) supplemented with 10% fetal bovine serum (FBS, Omega
526 Scientific), penicillin/streptomycin (Gibco), non-essential amino acids (Gibco) and L-glutamine
527 (Gibco) at 37C and 5% CO_2. HepG2-NTCP-K7 cells (Ko et al., 2018) (gift from Ulrike Protzer) and
528 HepAD38 cells (Ladner et al., 1997) (gift from Christoph Seeger) were cultured in DMEM/F12
529 (Gibco) supplemented with 10% FBS, penicillin/streptomycin, non-essential amino acids, L-
530 glutamine and sodium pyruvate (Gibco) at 37C and 5% CO_2. Cell lines were tested negative for
531 mycoplasma and were authenticated by STR profiling. Hepatitis A virus HM175/18f (NR-137) was
532 obtained through BEI Resources (NIAID, NIH) and HM175/clone 1 (VR-1541) through ATCC. HAV
533 strains were propagated in Huh7.5.1 cells grown in adeno expression media (Gibco)
534 supplemented with penicillin/streptomycin, non-essential amino acids and L-glutamine,
535 supernatant was collected 5-12 dpi and filtered (0.45 micron). To generate concentrated HAV
536 stocks, supernatant was incubated with 8% PEG-8000 at 4C overnight, centrifuged at 3,200g for
537 60min and pellet was resuspended in a small volume of DMEM with 10% FBS and aliquoted. For
538 the generation of HAV-Nluc (gift from Stanley Lemon) (Rivera-Serrano et al., 2019), the infectious
539 clone plasmid was linearized, RNA was *in-vitro* transcribed using MEGAscript T7 Transcription Kit
540 (Invitrogen) and transfected into Huh7.5.1 cells using TransIT-LT1 Transfection Reagent (Mirus
541 Bio). Subsequently, cell supernatant was collected 8-13dpi, filtered and aliquoted. Purified
542 encephalomyocarditis virus (NR-46441) was obtained through BEI Resources (NIAID, NIH).
543 Enterovirus 71 (MP4), rhinovirus A2 and HCV JFH1 stocks were kindly provided by Jan Carette.

544 For HBV production, supernatant was collected from HepAD38 cells, filtered (0.45 micron), and
545 concentrated using 8% PEG-8000 as described above. The HEV infectious clone (genotype 3) was
546 obtained from the NIH/NIAID and viral RNA was generated by *in-vitro* transcription from
547 linearized plasmid (Shukla et al., 2012). For virus stocks, titers were determined by plaque- or
548 focus-forming assay. RG7834 was purchased from MedKoo Biosciences and resuspended in
549 DMSO at 50mg/ml. Puromycin and blasticidin were obtained from Gibco.
550
551 CRISPR host factor screen
552 Huh7.5.1 cells were stably transduced with lentivirus from lentiCas9-Blast (Addgene #52962, gift
553 from Feng Zhang) and subsequently selected using blasticidin. Next, a total of 300 million
554 Huh7.5.1-Cas9 cells were then separately transduced with the lentiviral gRNA sublibraries A and
555 B of the human GeCKO v2 library (Addgene #1000000049, gift from Feng Zhang) at a multiplicity
556 of infection (MOI) of 0.3. Each sublibrary contained 3 guides per gene. Subsequently, the cells
557 were selected using puromycin and expanded for 10 days. A total of 60 million mutagenized cells
558 for each sublibrary (A and B) were collected for genomic DNA extraction, and a total of 45 million
559 mutagenized cells for each sublibrary were infected with 15ml of unconcentrated HAV
560 HM175/18f per T175 flask (1:1 diluted with fresh DMEM media). An additional 15ml of media
561 was added after 2h. Media was refreshed 4 and 8dpi and surviving cells were collected 12dpi for
562 genomic DNA extraction using QIAamp DNA Blood Maxi Kit (Qiagen). gRNA encoding DNA
563 sequences were amplified in a two-step nested PCR using KAPA HiFi HotStart ReadyMixPCR Kit
564 (Kapa Biosystems) and sequenced on an Illumina NextSeq (High Output) (for primer sequences,
565 see Supplementary Table 4). For analysis, reads were aligned to gRNA reference table and

566 enrichment of each gRNA was calculated by comparing the relative abundance in the selected
567 and unselected cell population. For screen analysis, the gRNA enrichment tables from the two
568 biological samples were merged to increase statistical power and RIGER analysis (using weighted
569 sum) as well as MaGeCK were performed to calculate gene significance (Li et al., 2014; Luo et al.,
570 2008). Gene ontology analysis of enriched genes in target list (containing 72 genes with RIGER p-
571 value < 0.001) was performed using GOrilla (Eden et al., 2009). No secondary validation screen
572 was performed.
573
574 Generation of clonal KO cell lines
575 Oligos containing gRNA sequence were annealed and ligated into pX458 (Addgene #48138, gift
576 from Feng Zhang). Cells were transfected with pX458 constructs using Lipofectamine 3000
577 (Invitrogen) and two days later GFP positive cells were single-cell sorted into 96-well plates using
578 a Sony SH800 cell sorter. For genotyping, genomic DNA was isolated from obtained clones using
579 QuickExtract (Lucigen), the gRNA-targeted sites PCR amplified and the products Sanger-
580 sequenced. Obtained sequences were compared to reference sequences for indel mutations or
581 large deletion. A list of all used gRNA oligo and genotyping primer sequences can be found in
582 Supplementary Table 4.
583
584 Intracellular RNA RT-qPCR assays
585 Cells were plated in 96-well plates (in triplicates for each condition) and infected the next day
586 with virus at the following MOIs: HAV (~5-10 FFU/cell), RV-A2 (~1 PFU/cell), EV-71 (~0.2 PFU/cell),
587 EMCV (~0.2 PFU/cell), HCV (~1 FFU/cell) and HBV (~1 FFU/cell). Cells were harvested, lysates

588 reverse transcribed and quantitative PCR performed on a Bio-Rad CFX96 Touch system using the
589 Power SYBR Cells-to-CT kit (Invitrogen). All viral RNA levels were normalized to 18S levels. Primer
590 sequences can be found in Supplementary file 1.
591
592 Quantification of extracellular viral RNA
593 Cells were plated in 96-well plates (duplicates for each condition) and infected with HAV at an
594 MOI of 5. After 4h, inoculum was removed and cells were washed with PBS. At 3 dpi 100µl of
595 supernatant was collected and RNA was isolated using the Qiagen Viral RNA Mini kit. Eluted RNA
596 was reversed transcribed and analyzed by qPCR as described above. For determination of
597 genome copies in-vitro transcribed HAV RNA was serially diluted and also quantified by RT-qPCR.
598
599 Viral attachment and entry assay
600 96-well plates containing WT, *SLC35A1* KO or *HAVCR1* KO Huh7.5.1 cells were chilled on ice
601 before infection with HAV HM175/18f at an MOI of 500 FFU/cell. Cells were incubated for 1h on
602 ice before moving them to a 37C incubator. At each harvest timepoint, cells were washed three
603 times with PBS and processed for RT-qPCR as described above.
604
605 HAV nanoluciferase reporter assay
606 Cells were plated in 96-well plates and infected the next day with equal amounts of HAV-Nluc.
607 Lysates were harvested by washing once with PBS wash followed by addition of 22µl of Passive
608 Lysis Buffer (Promega) under shaking for 15min. For luminescence readout, 15µl of lysate were
609 mixed with 50µl of Nano-Glo assay buffer (Promega) in a flat bottom white-walled luminescence

610 plate, incubated for 5min at room temperature and read on an EnVision plate reader
611 (PerkinElmer).
612
613 Complementation of KO cells with cDNA
614 UBA5 cDNA was obtained from Dharmacon (DNA Accession: BC009737, Clone ID: 3879061). To
615 generate cDNA encoding catalytically inactive enzyme, a Cys250Arg mutation was introduced by
616 PCR. Additionally, a C-terminal FLAG-tag was added to WT and CAT cDNA sequences. UFM1 was
617 obtained from Dharmacon (cDNA Accession: BC005193, Clone ID: 3829206). N-terminal FLAG and
618 C-terminal mutations (Gly83Ala or ΔC3 (deletion of GlySerCys)) were introduced by PCR. For
619 RPL26, cDNA was obtained from OriGene (RC209922) and a C-terminal FLAG-tag was added. To
620 introduce 5KR mutations, a reverse primer containing point 5 mutations was used. ZCCHC14
621 cDNA was obtained from Dharmacon (cDNA Accession: BC101478, Clone ID: 8068984). The N-
622 terminus was extended using a Gblock (Integrated DNA Technologies) resembling the protein
623 coding sequence for a longer isoform (1086 amino acids, ENST00000671377.1) to match the
624 molecular weight of ZCCHC14 detected in WT Huh7.5.1 by immunoblot. PCR products were gel-
625 purified and cloned into EcoRV-cut pLenti CMV Puro DEST (w118-1) (Addgene #17452, gift from
626 Eric Campeau & Paul Kaufman) using NEBuilder HiFi DNA Assembly Master Mix (New England
627 BioLabs). Lentivirus was produced in HEK293FT and collected 48h post-transfection. KO cells
628 were transduced with filtered, lentiviral containing supernatant under addition of polybrene and
629 selected using 4 µg/ml puromycin for 3-4 days. For PAPD5 and PAPD7, pCI3 plasmids with WT or
630 catalytic mutant cDNA sequences were kindly provided by V. Narry Kim and were described
631 previously (Lim et al., 2018). For transient complementation, plasmids were transfected into WT

632 or DKO cells using TransIT-LT1 Transfection Reagent (Mirus Bio), and transfected cells were
633 plated in 96-wells the next day for HAV infection. To generate stable cell lines, cDNA sequences
634 were cloned into the PB-CMV-MCS-EF1α-Puro vector (PB510B-1, SBI System Biosciences) where
635 the CMV promoter was replaced by a PGK promoter. Plasmids were co-transfected together with
636 a plasmid expressing piggyBac transposase into *PAPD5* KO cells, which were subsequently
637 selected with puromycin for 5 days starting 3 days post-transfection. All primer sequences can
638 be found in Supplementary file 1.
639
640 Immunoblotting
641 Cell were lysed using Laemmli SDS sample buffer containing 5% beta-mercaptoethanol and boiled
642 for 10min. Lysates were separated by SDS-PAGE on pre-cast Bio-Rad 4-15% poly-acrylamide gels
643 in Bio-Rad Mini-Protean electrophoresis system. Proteins were transferred onto PVDF
644 membranes using Bio-Rad Trans-Blot Turbo transfer system. PVDF membranes were blocked
645 with PBS buffer containing 0.1% Tween-20 and 5% non-fat milk. Blocked membranes were
646 incubated with primary antibody diluted in blocking buffer and incubated overnight at 4C on a
647 shaker. Primary antibodies were detected by incubating membranes with 1:4000 dilution of HRP-
648 conjugated (Southern Biotech) or 1:5000 dilution of IRDye-conjugated (LI-COR) secondary anti-
649 mouse and anti-rabbit antibodies for 1 h at room temperature. Blots were visualized using a
650 ChemiDoc MP Imaging System (Bio-Rad). The following primary antibodies (and their dilutions)
651 were used in this study: p84 (Genetex, GTX70220) at 1:1000, GAPDH (SCBT, sc-32233) at 1:1000,
652 vinculin (SCBT, sc-73614), 1:1000, eIF4B (SCBT, sc-376062) at 1:250, VPS4A (SCBT, sc-393428) at
653 1:300, SLC35A1 (Proteintech, 16342-1-AP) at 1:250, HAV VP1 (LS Bio, LS-C137674-100) at 1:1000,

654 FLAG M2 (Sigma, F1804) at 1:1000, UFM1 (Abcam, ab109305) at 1:1000, UBA5 (Bethyl, A304-
655 115A) at 1:2500, UFSP2 (SCBT, sc-376084) at 1:100, RPL26 (Bethyl, A300-686A) at 1:1000, PAPD5
656 (Atlas Antibodies, HPA042968) at 1:1000 and ZCCHC14 (Bethyl, A303-096A) at 1:1000. For
657 SLC35A1, lysates from 10^6 cells were immunoprecipitated using 4 µg anti-SLC35A1 antibody and
658 Protein G magnetic Dynabeads (Thermo Scientific, 10-003-D) overnight at 4C prior to
659 immunoblotting to enhance signal and specificity of signal.
660
661 Replicon assay
662 The replicon plasmids pLuc-HAV/18f and pLuc-HAV/18f-$3D^{pol}$GDD→GAA (replication-defective
663 mutant) were kindly provided by Stanley Lemon and were described previously (González-López
664 et al., 2018). Plasmids were linearized using MluI-HF (New England BioLabs), RNA was generated
665 using the MEGAscript T7 Kit (Invitrogen) and subsequently purified by lithium chloride
666 precipitation. For electroporation, 1-2 million cells were washed three times in PBS, resuspended
667 in 100µl SF Nucleofector solution (Lonza), mixed with 250ng replicon RNA per 80k cells,
668 transferred to a 100 µl nucleocuvette and pulsed using the program FF-137 on an Amaxa 4D-
669 Nucleofector X Unit (Lonza). Cells were then resuspended in equilibrated, antibiotic-free
670 medium, distributed into 96-wells and lysed at different timepoints post-electroporation using
671 40µl Passive Lysis buffer (Promega). Luminescence was measured using Luciferase Assay System
672 (Promega) on a white-walled luminescence plate with an EnVision plate reader (PerkinElmer).
673
674 Poly(A) tail length assay by polyacrylamide gel electrophoresis

675 Cells were infected with HAV HM175/18f (MOI=10) and harvested 3 days post-infection using
676 Trizol (Invitrogen). RNA was purified with Direct-zol RNA Microprep columns (Zymo Research).
677 HAV poly(A) tails were analyzed using the Poly(A) Tail-Length Assay Kit (Thermo Scientific)
678 according to the manufacturer's instructions. Briefly, 1µg total RNA per condition was used as
679 input for G/I tailing reaction followed by reverse transcription. Next, RT products were amplified
680 using different PCR primer combinations: i) HAV genome-specific (GS) forward and GS reverse
681 primer, ii) GS forward and G/I reverse primer and iii) forward primer upstream of HAV poly(A)
682 start site and G/I reverse primer. Similarly, for HBV, cDNA was amplified by either a GS primer
683 pair or the GS forward primer with the G/I reverse primer. PCR products were analyzed using
684 polyacrylamide gel electrophoresis on a 5% Mini-PROTEAN Tris/Boric Acid/EDTA (TBE) gel in TBE
685 buffer (100V for 60min). Gel was stained with SYBR Gold (diluted 1:10000 in TBE buffer) for
686 ~30min in the dark and imaged on a ChemiDoc MP Imaging System (Bio-Rad).
687
688 Poly(A) tail sequencing
689 RNA was isolated from infected cells as described above. Ribosomal RNA (rRNA) was depleted
690 from 1µg total RNA by addition of rRNA Removal Mix – Gold (Illumina) followed by incubation at
691 68C for 5min, addition of rRNA Removal Beads (Illumina), removal of supernatant while tubes
692 are on a magnetic rack, and finally elution of rRNA-depleted RNA. Next, a 5´ adenylated, 3´
693 blocked oligodeoxynucleotide RNA linker (S1315S, New England BioLabs) was ligated to the 3'
694 ends of RNAs by incubation with RNA ligase 2, truncated (New England BioLabs) for 3h at 22C.
695 Ligation products were then reverse transcribed using a primer, which is reverse complement to
696 the RNA linker, and Superscript IV (Invitrogen). Finally, HAV poly(A) tails were specifically

697 amplified in a nested PCR, cloned into the pCRBlunt II-TOPO vector (Invitrogen) and Sanger
698 sequenced (Quintarabio). Number of adenosines downstream of the HAV 3'UTR region and
699 occurrence of non-adenosine nucleotides were counted.
700
701 Tapestation analysis of poly(A) tails of replicon RNA
702 10^6 cells were electroporated with *in-vitro* transcribed replicon RNA containing a 40bp long
703 poly(A) tail as described above. For each timepoint, cells were washed with PBS, trypsinized,
704 pelleted and lysed using Trizol followed by RNA extraction with Direct-zol columns. Total RNA
705 was G/I tailed, reverse transcribed and poly(A) tail region was amplified using forward primer
706 upstream of HAV poly(A) start site and G/I reverse primer. Products were analyzed using a High
707 Sensitivity D1000 ScreenTape System (Agilent).
708
709 EU pulse-chase assay
710 WT or *PAPD7* KO cells were plated in 12-well plates and infected with HAV. After 48h media was
711 changed to DMEM containing 100 µM 5-ethynyl uridine (EU) and cultured for 16h to label all
712 nascent RNAs. Additionally, 1 µM RG7834 was added to *PAPD7* KO cells to mimic the DKO
713 phenotype. At t=0h of the chase, EU containing media was replaced to DMEM without EU but
714 still containing RG7834 in the *PAPD7* KO wells. At each timepoint cells were harvested in Trizol
715 and total RNA was extracted. To capture EU labeled RNA, the Click-iT® Nascent RNA Capture Kit
716 (Thermo Scientific, C10365) was used. Briefly, 1.5 µg input RNA was used for the click-based
717 biotinylation. Next, RNA was precipitated and resuspended in 35 µl. 20 µl of biotinylated RNA
718 were added to 16 µl of Dynabeads® MyOneTM Streptavidin T1 and incubated for 1h. After

719 washes, beads were resuspended in 16 µl wash buffer and used as template for reverse
720 transcription. Finally, Dynabeads were removed from resulting cDNA and qPCR was performed.
721
722 Cell viability assay
723 Huh7.5.1 cells were treated with different concentrations of RG7834 for 3 days and viability was
724 measured using Cell Titer Glo (Promega) according to the manufacturer's instructions.
725
726 Culture and HAV infection of human liver organoids
727 Bi-potent stem cell organoids were generated as previously described (Broutier et al., 2016; Huch
728 et al., 2015). Briefly, liver tissue samples from healthy resection margins of partial hepatectomies
729 were obtained through the Ibrahim El-Hefni Liver Biorepository at the California Pacific Medical
730 Center Research Institute. Following tissue digest, the heterogeneous mixture of single cells was
731 suspended in reduced growth factor BME2 (Basement Membrane Extract, Type 2, Trevigen).
732 From this mixture, 50 µL drops containing 1,000 to 20,000 cells were seeded in 24-well
733 suspension culture plates (GreinerBio). Drops were incubated at 37C for >20 min and solidified.
734 After this, 500 µL of expansion media (EM) was added to each well. Expansion media is basal
735 media (Advanced DMEM/F12 with 1% penicillin/streptomycin, 1% Glutamax, and 10 mM HEPES
736 (all from ThermoFisher) supplemented with 1% N2 (Gibco), 1% B27 (Gibco), 1 mM N-
737 Acetylcysteine (Sigma-Aldrich), 10 nM [Leu^{15}]-gastrin I human (Sigma-Aldrich), 10% (vol/vol) R-
738 spondin1 conditioned media (generated as described in (Broutier et al., 2016)), and 10 mM
739 Nicotinamide (Sigma-Aldrich). Expansion media additionally contains 50 ng/ml recombinant
740 human EGF, 25 ng/ml recombinant human HGF, 100 ng/ml recombinant human FGF10, 10 µM

741 Forskolin, and 5 µM A83-01 (all from Stem Cell Technologies). Expansion media was replaced
742 every 3-4 days. Organoids in expansion media grew in culture for 4-6 months and needed to be
743 routinely passaged with TRYPLE (Gibco). To induce differentiation to a hepatocyte-like fate,
744 expansion media was supplemented with 25 ng/ml BMP7 (ProSpec) for 3-4 days. After this, media
745 was changed to differentiation media (DM). Differentiation media is basal media supplemented
746 with 1% N2, 1% B27, 1 mM N-acetylcysteine, 10 nM [Leu^{15}]-gastrin I human, 50 ng/ml EGF, 25
747 ng/ml HGF, 0.5 µM A83-01, 25 ng/ml BMP7, 3 µM dexamethasone (Sigma-Aldrich), 10 µM DAPT
748 (Stem Cell Technologies), and 100 ng/ml recombinant human FGF19 (ProSpec). Differentiation
749 media was changed every 3-4 days for a period of 3-15 days. For HAV infection, organoid lines
750 from two non-viral donors were spin-infected with the HM175/18f strain of HAV as follows.
751 Organoids from EM and DM d3 conditions were collected and lightly dissociated by a 3 min
752 incubation at 37°C with TRYPLE. Cells were then suspended in basal media containing 10 µM Y-
753 27632 (Stem Cell Technologies) and counted. These cells were mixed with HAV at an MOI of 500
754 FFU/cell in the presence and absence of RG7834 at 100 or 500 nM. Cell suspensions were then
755 added to a 24-well suspension culture plate. The plate was centrifuged at 600 x g for 1 h at room
756 temperature, followed by a 2 h incubation at 37C. After this, cells were collected and washed 3x
757 in basal media. Washed cells were seeded in fresh BME2 drops in a new 24-well suspension
758 culture plate. At 7 days post-infection, infected organoid samples were washed 2x in cold basal
759 media, and cell pellets were lysed in Trizol.
760
761 <u>Generation of phylogenetic tree</u>

762 Whole viral genome sequences for HAV (KP879216), HCV (EU363761), EV-D68 (KU509997), EV-
763 71 (AB204853), RV-A2 (MN228695), RV-C15 (MG881840) and EMCV (KP892662) were aligned
764 using the Geneious Prime Tree Builder based on the Tamura-Nei genetic distance model.
765
766 Statistical analysis
767 Prism 8 (GraphPad Software) was used for statistical analysis. Statistical tests and p-value
768 definitions are listed in the figure legends.
769
770 **Supplementary files**
771 Supplementary file 1: Oligo sequences.
772
773 **Data availability**
774 Raw sequencing data for CRISPR KO screen is deposited at the EMBL-EBI ArrayExpress
775 (https://www.ebi.ac.uk/arrayexpress/) under the accession number E-MTAB-8646.
776
777 **Author contributions**
778 JK and ASP were responsible for design and execution of experiments, data analysis and
779 manuscript preparation. RW performed comparative analysis of CRISPR screens and assisted with
780 molecular biology experiments. NLM conducted organoid experiments under the supervision of
781 MO. ASP conceptualized and supervised the study.
782
783 **Acknowledgments**

784 We would like to thank Don Ganem for helpful discussions and critically reading the manuscript,
785 the Biohub Genomics platform for help with sequencing, James Webber for assistance with the
786 CRISPR screen analysis, and members of the Biohub Infectious Disease Initiative for helpful
787 discussions. We would like to acknowledge Drs. Stanley Lemon (University of North Carolina,
788 Chapel Hill), Jan Carette (Stanford University), V. Narry Kim (Seoul National University), Ron
789 Kopito (Stanford University), Ulrike Protzer (Technical University Munich), Feng Zhang (Broad
790 Institute), Christoph Seeger (Fox Chase Cancer Center) and Suzanne Emerson (NIH) for providing
791 critical reagents. We also acknowledge Drs. Stewart Cooper and Ann Erickson, who oversee the
792 Ibrahim El-Hefni Liver Biorepository at the California Pacific Medical Center Research Institute
793 and provided patient tissue samples used to generate liver organoids. The research was funded
794 by the Chan Zuckerberg Biohub (ASP) and by NIH/NIDA grants AI097552 and DP1DA038043-01
795 (MO).
796
797

798 **References**

799 Avanzino BC, Fuchs G, Fraser CS. 2017. Cellular cap-binding protein, eIF4E, promotes
800 picornavirus genome restructuring and translation. *Proc Natl Acad Sci* **114**:9611–9616.
801 doi:10.1073/pnas.1704390114

802 Baggen J, Thibaut HJ, Staring J, Jae LT, Liu Y, Guo H, Slager JJ, Bruin JW de, Vliet ALW van,
803 Blomen VA, Overduin P, Sheng J, Haan CAM de, Vries E de, Meijer A, Rossmann MG,
804 Brummelkamp TR, Kuppeveld FJM van. 2016. Enterovirus D68 receptor requirements
805 unveiled by haploid genetics. *Proc Natl Acad Sci* **113**:1399–1404.
806 doi:10.1073/pnas.1524498113

807 Berndt H, Harnisch C, Rammelt C, Stöhr N, Zirkel A, Dohm JC, Himmelbauer H, Tavanez J-P,
808 Hüttelmaier S, Wahle E. 2012. Maturation of mammalian H/ACA box snoRNAs:
809 PAPD5-dependent adenylation and PARN-dependent trimming. *RNA* **18**:958–972.
810 doi:10.1261/rna.032292.112

811 Boele J, Persson H, Shin JW, Ishizu Y, Newie IS, Søkilde R, Hawkins SM, Coarfa C, Ikeda K,
812 Takayama K, Horie-Inoue K, Ando Y, Burroughs AM, Sasaki C, Suzuki C, Sakai M,
813 Aoki S, Ogawa A, Hasegawa A, Lizio M, Kaida K, Teusink B, Carninci P, Suzuki H,
814 Inoue S, Gunaratne PH, Rovira C, Hayashizaki Y, de Hoon MJL. 2014. PAPD5-mediated
815 3' adenylation and subsequent degradation of miR-21 is disrupted in proliferative disease.
816 *Proc Natl Acad Sci U S A* **111**:11467–11472. doi:10.1073/pnas.1317751111

817 Borman AM, Michel YM, Kean KM. 2001. Detailed Analysis of the Requirements of Hepatitis
818 A Virus Internal Ribosome Entry Segment for the Eukaryotic Initiation Factor Complex
819 eIF4F. *J Virol* **75**:7864–7871. doi:10.1128/JVI.75.17.7864-7871.2001

820 Broutier L, Andersson-Rolf A, Hindley CJ, Boj SF, Clevers H, Koo B-K, Huch M. 2016. Culture
821 and establishment of self-renewing human and mouse adult liver and pancreas 3D
822 organoids and their genetic manipulation. *Nat Protoc* **11**:1724–1743.
823 doi:10.1038/nprot.2016.097
824 CDC. 2019. Widespread person-to-person outbreaks of hepatitis A across the United States |
825 CDC. https://www.cdc.gov/hepatitis/outbreaks/2017March-HepatitisA.htm
826 Chen C, Itakura E, Weber KP, Hegde RS, de Bono M. 2014. An ER complex of ODR-4 and
827 ODR-8/Ufm1 specific protease 2 promotes GPCR maturation by a Ufm1-independent
828 mechanism. *PLoS Genet* **10**:e1004082. doi:10.1371/journal.pgen.1004082
829 Das A, Hirai-Yuki A, González-López O, Rhein B, Moller-Tank S, Brouillette R, Hensley L,
830 Misumi I, Lovell W, Cullen JM, Whitmire JK, Maury W, Lemon SM. 2017. TIM1
831 (HAVCR1) Is Not Essential for Cellular Entry of Either Quasi-enveloped or Naked
832 Hepatitis A Virions. *mBio* **8**. doi:10.1128/mBio.00969-17
833 Diep J, Ooi YS, Wilkinson AW, Peters CE, Foy E, Johnson JR, Zengel J, Ding S, Weng K-F,
834 Laufman O, Jang G, Xu J, Young T, Verschueren E, Kobluk KJ, Elias JE, Sarnow P,
835 Greenberg HB, Hüttenhain R, Nagamine CM, Andino R, Krogan NJ, Gozani O, Carette
836 JE. 2019. Enterovirus pathogenesis requires the host methyltransferase SETD3. *Nat*
837 *Microbiol*. doi:10.1038/s41564-019-0551-1
838 Ding S, Diep J, Feng N, Ren L, Li B, Ooi YS, Wang X, Brulois KF, Yasukawa LL, Li X, Kuo
839 CJ, Solomon DA, Carette JE, Greenberg HB. 2018. STAG2 deficiency induces interferon
840 responses via cGAS-STING pathway and restricts virus infection. *Nat Commun* **9**:1–8.
841 doi:10.1038/s41467-018-03782-z

842 Drake MJ, Brennan B, Jr KB, Bart SM, Sherman E, Szemiel AM, Minutillo M, Bushman FD,
843 Bates P. 2017. A role for glycolipid biosynthesis in severe fever with thrombocytopenia
844 syndrome virus entry. *PLOS Pathog* **13**:e1006316. doi:10.1371/journal.ppat.1006316
845 Eden E, Navon R, Steinfeld I, Lipson D, Yakhini Z. 2009. GOrilla: a tool for discovery and
846 visualization of enriched GO terms in ranked gene lists. *BMC Bioinformatics* **10**:48.
847 doi:10.1186/1471-2105-10-48
848 Feng Z, Hensley L, McKnight KL, Hu F, Madden V, Ping L, Jeong S-H, Walker C, Lanford RE,
849 Lemon SM. 2013. A pathogenic picornavirus acquires an envelope by hijacking cellular
850 membranes. *Nature* **496**:367–371. doi:10.1038/nature12029
851 Gerakis Y, Quintero M, Li H, Hetz C. 2019. The UFMylation System in Proteostasis and
852 Beyond. *Trends Cell Biol* **29**:974–986. doi:10.1016/j.tcb.2019.09.005
853 Go CD, Knight JDR, Rajasekharan A, Rathod B, Hesketh GG, Abe KT, Youn J-Y, Samavarchi-
854 Tehrani P, Zhang H, Zhu LY, Popiel E, Lambert J-P, Coyaud É, Cheung SWT,
855 Rajendran D, Wong CJ, Antonicka H, Pelletier L, Raught B, Palazzo AF, Shoubridge
856 EA, Gingras A-C. 2019. A proximity biotinylation map of a human cell. *bioRxiv* 796391.
857 doi:10.1101/796391
858 González-López O, Rivera-Serrano EE, Hu F, Hensley L, McKnight KL, Ren J, Stuart DI, Fry
859 EE, Lemon SM. 2018. Redundant Late Domain Functions of Tandem VP2 YPX3L
860 Motifs in Nonlytic Cellular Egress of Quasi-enveloped Hepatitis A Virus. *J Virol* **92**.
861 doi:10.1128/JVI.01308-18
862 Gosert R, Chang KH, Rijnbrand R, Yi M, Sangar DV, Lemon SM. 2000. Transient expression of
863 cellular polypyrimidine-tract binding protein stimulates cap-independent translation

864 directed by both picornaviral and flaviviral internal ribosome entry sites In vivo. *Mol Cell*
865 *Biol* **20**:1583–1595. doi:10.1128/mcb.20.5.1583-1595.2000
866 Hamill S, Wolin SL, Reinisch KM. 2010. Structure and function of the polymerase core of
867 TRAMP, a RNA surveillance complex. *Proc Natl Acad Sci U S A* **107**:15045–15050.
868 doi:10.1073/pnas.1003505107
869 Han J, Perez JT, Chen C, Li Y, Benitez A, Kandasamy M, Lee Y, Andrade J, tenOever B,
870 Manicassamy B. 2018. Genome-wide CRISPR/Cas9 Screen Identifies Host Factors
871 Essential for Influenza Virus Replication. *Cell Rep* **23**:596–607.
872 doi:10.1016/j.celrep.2018.03.045
873 Huch M, Gehart H, van Boxtel R, Hamer K, Blokzijl F, Verstegen MMA, Ellis E, van Wenum
874 M, Fuchs SA, de Ligt J, van de Wetering M, Sasaki N, Boers SJ, Kemperman H, de
875 Jonge J, Ijzermans JNM, Nieuwenhuis EES, Hoekstra R, Strom S, Vries RRG, van der
876 Laan LJW, Cuppen E, Clevers H. 2015. Long-term culture of genome-stable bipotent
877 stem cells from adult human liver. *Cell* **160**:299–312. doi:10.1016/j.cell.2014.11.050
878 Hyrina A, Jones C, Chen D, Clarkson S, Cochran N, Feucht P, Hoffman G, Lindeman A, Russ C,
879 Sigoillot F, Tsang T, Uehara K, Xie L, Ganem D, Holdorf M. 2019. A Genome-wide
880 CRISPR Screen Identifies ZCCHC14 as a Host Factor Required for Hepatitis B Surface
881 Antigen Production. *Cell Rep* **29**:2970-2978.e6. doi:10.1016/j.celrep.2019.10.113
882 Jacobsen KH. 2018. Globalization and the Changing Epidemiology of Hepatitis A Virus. *Cold*
883 *Spring Harb Perspect Med* **8**:a031716. doi:10.1101/cshperspect.a031716
884 Kang SH, Kim GR, Seong M, Baek SH, Seol JH, Bang OS, Ovaa H, Tatsumi K, Komatsu M,
885 Tanaka K, Chung CH. 2007. Two novel ubiquitin-fold modifier 1 (Ufm1)-specific
886 proteases, UfSP1 and UfSP2. *J Biol Chem* **282**:5256–5262. doi:10.1074/jbc.M610590200

887 Kaplan G, Totsuka A, Thompson P, Akatsuka T, Moritsugu Y, Feinstone SM. 1996.
888 Identification of a surface glycoprotein on African green monkey kidney cells as a
889 receptor for hepatitis A virus. *EMBO J* **15**:4282–4296.
890 Kempf BJ, Kelly MM, Springer CL, Peersen OB, Barton DJ. 2013. Structural features of a
891 picornavirus polymerase involved in the polyadenylation of viral RNA. *J Virol* **87**:5629–
892 5644. doi:10.1128/JVI.02590-12
893 Ko C, Chakraborty A, Chou W-M, Hasreiter J, Wettengel JM, Stadler D, Bester R, Asen T,
894 Zhang K, Wisskirchen K, McKeating JA, Ryu W-S, Protzer U. 2018. Hepatitis B virus
895 genome recycling and de novo secondary infection events maintain stable cccDNA
896 levels. *J Hepatol* **69**:1231–1241. doi:10.1016/j.jhep.2018.08.012
897 Komatsu M, Chiba T, Tatsumi K, Iemura S, Tanida I, Okazaki N, Ueno T, Kominami E,
898 Natsume T, Tanaka K. 2004. A novel protein-conjugating system for Ufm1, a ubiquitin-
899 fold modifier. *EMBO J* **23**:1977–1986. doi:10.1038/sj.emboj.7600205
900 Ladner SK, Otto MJ, Barker CS, Zaifert K, Wang GH, Guo JT, Seeger C, King RW. 1997.
901 Inducible expression of human hepatitis B virus (HBV) in stably transfected
902 hepatoblastoma cells: a novel system for screening potential inhibitors of HBV
903 replication. *Antimicrob Agents Chemother* **41**:1715–1720.
904 Landry DM, Hertz MI, Thompson SR. 2009. RPS25 is essential for translation initiation by the
905 Dicistroviridae and hepatitis C viral IRESs. *Genes Dev* **23**:2753–2764.
906 doi:10.1101/gad.1832209
907 Lemon SM, Murphy PC, Shields PA, Ping LH, Feinstone SM, Cromeans T, Jansen RW. 1991.
908 Antigenic and genetic variation in cytopathic hepatitis A virus variants arising during
909 persistent infection: evidence for genetic recombination. *J Virol* **65**:2056–2065.

910 Li W, Xu H, Xiao T, Cong L, Love MI, Zhang F, Irizarry RA, Liu JS, Brown M, Liu XS. 2014.
911 MAGeCK enables robust identification of essential genes from genome-scale
912 CRISPR/Cas9 knockout screens. *Genome Biol* **15**:554. doi:10.1186/s13059-014-0554-4
913 Lim J, Kim D, Lee Y-S, Ha M, Lee M, Yeo J, Chang H, Song J, Ahn K, Kim VN. 2018. Mixed
914 tailing by TENT4A and TENT4B shields mRNA from rapid deadenylation. *Science*
915 **361**:701–704. doi:10.1126/science.aam5794
916 Lubas M, Christensen MS, Kristiansen MS, Domanski M, Falkenby LG, Lykke-Andersen S,
917 Andersen JS, Dziembowski A, Jensen TH. 2011. Interaction Profiling Identifies the
918 Human Nuclear Exosome Targeting Complex. *Mol Cell* **43**:624–637.
919 doi:10.1016/j.molcel.2011.06.028
920 Luo B, Cheung HW, Subramanian A, Sharifnia T, Okamoto M, Yang X, Hinkle G, Boehm JS,
921 Beroukhim R, Weir BA, Mermel C, Barbie DA, Awad T, Zhou X, Nguyen T, Piqani B,
922 Li C, Golub TR, Meyerson M, Hacohen N, Hahn WC, Lander ES, Sabatini DM, Root
923 DE. 2008. Highly parallel identification of essential genes in cancer cells. *Proc Natl Acad*
924 *Sci U S A* **105**:20380–20385. doi:10.1073/pnas.0810485105
925 Majzoub K, Hafirassou ML, Meignin C, Goto A, Marzi S, Fedorova A, Verdier Y, Vinh J,
926 Hoffmann JA, Martin F, Baumert TF, Schuster C, Imler J-L. 2014. RACK1 controls
927 IRES-mediated translation of viruses. *Cell* **159**:1086–1095.
928 doi:10.1016/j.cell.2014.10.041
929 Marceau CD, Puschnik AS, Majzoub K, Ooi YS, Brewer SM, Fuchs G, Swaminathan K, Mata
930 MA, Elias JE, Sarnow P, Carette JE. 2016. Genetic dissection of Flaviviridae host factors
931 through genome-scale CRISPR screens. *Nature* **535**:159–163. doi:10.1038/nature18631

932 McKnight KL, Lemon SM. 2018. Hepatitis A Virus Genome Organization and Replication
933 Strategy. *Cold Spring Harb Perspect Med* a033480. doi:10.1101/cshperspect.a033480
934 Mueller H, Lopez A, Tropberger P, Wildum S, Schmaler J, Pedersen L, Han X, Wang Y, Ottosen
935 S, Yang S, Young JAT, Javanbakht H. 2019. PAPD5/7 Are Host Factors That Are
936 Required for Hepatitis B Virus RNA Stabilization. *Hepatology* **69**:1398–1411.
937 doi:10.1002/hep.30329
938 Mueller H, Wildum S, Luangsay S, Walther J, Lopez A, Tropberger P, Ottaviani G, Lu W,
939 Parrott NJ, Zhang JD, Schmucki R, Racek T, Hoflack J-C, Kueng E, Point F, Zhou X,
940 Steiner G, Lütgehetmann M, Rapp G, Volz T, Dandri M, Yang S, Young JAT,
941 Javanbakht H. 2018. A novel orally available small molecule that inhibits hepatitis B
942 virus expression. *J Hepatol* **68**:412–420. doi:10.1016/j.jhep.2017.10.014
943 Nousch M, Yeroslaviz A, Habermann B, Eckmann CR. 2014. The cytoplasmic poly(A)
944 polymerases GLD-2 and GLD-4 promote general gene expression via distinct
945 mechanisms. *Nucleic Acids Res* **42**:11622–11633. doi:10.1093/nar/gku838
946 Pestova TV, Hellen CU, Shatsky IN. 1996. Canonical eukaryotic initiation factors determine
947 initiation of translation by internal ribosomal entry. *Mol Cell Biol* **16**:6859–6869.
948 doi:10.1128/MCB.16.12.6859
949 Rammelt C, Bilen B, Zavolan M, Keller W. 2011. PAPD5, a noncanonical poly(A) polymerase
950 with an unusual RNA-binding motif. *RNA* **17**:1737–1746. doi:10.1261/rna.2787011
951 Rivera-Serrano EE, González-López O, Das A, Lemon SM. 2019. Cellular entry and uncoating
952 of naked and quasi-enveloped human hepatoviruses. *eLife* **8**:e43983.
953 doi:10.7554/eLife.43983

954 Schmid M, Jensen TH. 2018. Controlling nuclear RNA levels. *Nat Rev Genet* **19**:518–529.
955 doi:10.1038/s41576-018-0013-2
956 Shcherbik N, Wang M, Lapik YR, Srivastava L, Pestov DG. 2010. Polyadenylation and
957 degradation of incomplete RNA polymerase I transcripts in mammalian cells. *EMBO Rep*
958 **11**:106–111. doi:10.1038/embor.2009.271
959 Shin J, Paek KY, Ivshina M, Stackpole EE, Richter JD. 2017. Essential role for non-canonical
960 poly(A) polymerase GLD4 in cytoplasmic polyadenylation and carbohydrate metabolism.
961 *Nucleic Acids Res* **45**:6793–6804. doi:10.1093/nar/gkx239
962 Shukla P, Nguyen HT, Faulk K, Mather K, Torian U, Engle RE, Emerson SU. 2012. Adaptation
963 of a genotype 3 hepatitis E virus to efficient growth in cell culture depends on an inserted
964 human gene segment acquired by recombination. *J Virol* **86**:5697–5707.
965 doi:10.1128/JVI.00146-12
966 Spector DH, Baltimore D. 1975. Polyadenylic acid on poliovirus RNA: IV. Poly(U) in
967 replicative intermediate and double-stranded RNA. *Virology* **67**:498–505.
968 doi:10.1016/0042-6822(75)90450-X
969 Steil BP, Kempf BJ, Barton DJ. 2010. Poly(A) at the 3′ End of Positive-Strand RNA and VPg-
970 Linked Poly(U) at the 5′ End of Negative-Strand RNA Are Reciprocal Templates during
971 Replication of Poliovirus RNA. *J Virol* **84**:2843–2858. doi:10.1128/JVI.02620-08
972 Tatsumi K, Sou Y, Tada N, Nakamura E, Iemura S, Natsume T, Kang SH, Chung CH, Kasahara
973 M, Kominami E, Yamamoto M, Tanaka K, Komatsu M. 2010. A novel type of E3 ligase
974 for the Ufm1 conjugation system. *J Biol Chem* **285**:5417–5427.
975 doi:10.1074/jbc.M109.036814

976 Vaňáčová Š, Wolf J, Martin G, Blank D, Dettwiler S, Friedlein A, Langen H, Keith G, Keller W.
977 2005. A New Yeast Poly(A) Polymerase Complex Involved in RNA Quality Control.
978 *PLOS Biol* **3**:e189. doi:10.1371/journal.pbio.0030189
979 Votteler J, Sundquist WI. 2013. Virus Budding and the ESCRT Pathway. *Cell Host Microbe*
980 **14**:232–241. doi:10.1016/j.chom.2013.08.012
981 Walczak CP, Leto DE, Zhang L, Riepe C, Muller RY, DaRosa PA, Ingolia NT, Elias JE, Kopito
982 RR. 2019. Ribosomal protein RPL26 is the principal target of UFMylation. *Proc Natl*
983 *Acad Sci U S A* **116**:1299–1308. doi:10.1073/pnas.1816202116
984 Wang L, Xu Y, Rogers H, Saidi L, Noguchi CT, Li H, Yewdell JW, Guydosh NR, Ye Y. 2019.
985 UFMylation of RPL26 links translocation-associated quality control to endoplasmic
986 reticulum protein homeostasis. *Cell Res*. doi:10.1038/s41422-019-0236-6
987 Warkocki Z, Liudkovska V, Gewartowska O, Mroczek S, Dziembowski A. 2018. Terminal
988 nucleotidyl transferases (TENTs) in mammalian RNA metabolism. *Philos Trans R Soc B*
989 *Biol Sci* **373**:20180162. doi:10.1098/rstb.2018.0162
990 Wu J, Lei G, Mei M, Tang Y, Li H. 2010. A novel C53/LZAP-interacting protein regulates
991 stability of C53/LZAP and DDRGK domain-containing Protein 1 (DDRGK1) and
992 modulates NF-kappaB signaling. *J Biol Chem* **285**:15126–15136.
993 doi:10.1074/jbc.M110.110619
994 Zhang R, Miner JJ, Gorman MJ, Rausch K, Ramage H, White JP, Zuiani A, Zhang P, Fernandez
995 E, Zhang Q, Dowd KA, Pierson TC, Cherry S, Diamond MS. 2016. A CRISPR screen
996 defines a signal peptide processing pathway required by flaviviruses. *Nature* **535**:164–
997 168. doi:10.1038/nature18625
998